Exploration of Subjective Color Perceptual-Ability by EEG-Induced Type-2 Fuzzy Classifiers

Mousumi Laha, Amit Konar, Pratyusha Rakshit, and Atulya K. Nagar

***Abstract*— Perceptual-ability informally refers to the ability of a person to recognize a stimulus. This paper deals with color perceptual-ability measurement of subjects using brain response to basic color (red, green and blue) stimuli. It also attempts to determine subjective ability to recognize the base colors in presence of noise tolerance of the base colors, referred to as recognition tolerance. Because of intra- and inter-session variations in subjective brain signal features for a given color stimulus, there exists uncertainty in perceptual-ability. In addition, small variations in the color stimulus result in wide variations in brain signal features, introducing uncertainty in perceptual-ability of the subject.**

Type-2 fuzzy logic has been employed to handle the uncertainty in color perceptual-ability measurements due to a) variations in brain signal features for a given color, and b) the presence of colored noise on the base colors. Because of limited power of uncertainty management of interval type-2 fuzzy sets and high computational overhead of its general type-2 counterpart, we developed a semi-general type-2 fuzzy classifier to recognize the base color. It is important to note that the proposed technique transforms a vertical slice based general type-2 fuzzy set into an equivalent interval type-2 counterpart to reduce the computational overhead, without losing the contributions of the secondary memberships. The proposed semi-general type-2 fuzzy sets induced classifier yields superior performance in classification accuracy with respect to existing type-1, type-2 and other well-known classifiers. The brain-understanding of a perceived base or noisy base colors is also obtained by exact low resolution electromagnetic topographic analysis (e-LORETA) software. This is used as the reference for our experimental results of the semi-general type-2 classifier in color perceptual-ability detection. Statistical tests undertaken confirm the superiority of the proposed classifier over its competitors. The proposed technique is expected to have interesting applications in identifying people with excellent color perceptual-ability for chemical, pharmaceutical and textile industries.

***Index Terms*— color perceptual-ability, type-2 fuzzy sets, type-2 fuzzy classifiers, e-LORETA.**

I. Introduction

Like most of the mammals, humans too process light stimuli by rod cells and color stimuli by cone cells present in the retina of their eyes [1]. Although color perceptual-ability is apparently a well-understood term, unfortunately it lacks a formal definition. In this paper, color perceptual-ability is defined as the composite ability of a subject i) to recognize the base colors (red/green/blue) and ii) also to discriminate a given base color in presence of color noise [2]. This paper aims at measuring color perceptual-ability of human subjects by attempting to determine the above two parameters experimentally using an electroencephalography (EEG) based brain-computer interfacing (BCI) system [3].

Although sensitivity of primary colors (red/green/blue) by three different types of cone cells [4], [5] is already established, unfortunately there is hardly any supporting evidence on the activation of different brain regions for different color stimuli. This paper proposes a 2-step approach to fill this void. In the first step, EEG signals are acquired from the electrodes placed over the entire scalp with spacing following the standard 10-20 system [6]. The activation of different brain lobes due to a given color stimulus is determined using the e-LORETA software [7]. The e-LORETA identifies the most active regions/lobes in the brain during the perceptual process of a given colored stimulus [8]. In the second step, EEG signals are captured from the active brain lobes/regions for 1000ms to classify the perceived color. This time-interval of 1000ms is good enough to collect the brain-response to color stimuli.

Existing works on color perception are concerned with determining the effective frequency bands [9], [10] for color stimuli processing by the human brain. Experiments undertaken by different research groups reveal that the lower alpha and upper theta bands are responsible for color perception. Franklin, in an interesting work [11] correlates colored light with memory gain of autistic children and reports an enhancement in non-verbal ability of those children in presence of colored light. In addition, in [12], [13], the authors demonstrate improved memory performance of learners by EEG analysis of the colored light response of the brain. Viola in [14] asserts that blue enriched white light improves both subjective alertness and fatigue. Sur emphasizes [15] the role of the posterior parietal cortex (PPC) in controlling the sensory modality in complex sensory-motor decision-making tasks

In early stage of our research, we noticed that the brain response to individual color of a subject varies widely over experimental sessions comprising a fixed number of experimental trials. This in turn causes significant variation in the extracted feature values of the EEG across different sessions. Besides, small variations (noise) in the color stimulus yield wider variations in EEG features, resulting in uncertainty in perceptual-ability of the subject. Type-2 fuzzy set has an inherent characteristic of handling wide variation in individual features [16], [17]. This inspired us to employ type-2 fuzzy sets for the classification of color stimuli from the brain response of the subjects. Two common varieties of

type-2 fuzzy sets are popularly used in the literature. They are often referred to as interval type-2 fuzzy sets (IT2FS) [18] and general type-2 fuzzy sets (GT2FS) [19]. IT2FS may be regarded as a special case of a GT2FS with all secondary membership functions (MFs) equal to one. So, usually, the secondary membership functions are not used in IT2FS-based fuzzy reasoning. In GT2FS-based reasoning, we, however, utilize both primary and secondary membership functions to derive fuzzy inferences. Because of the involvement of both primary and secondary membership functions, the GT2FS-based reasoning often yields better performance unlike its interval type-2 counterpart, however at the cost of excessive computational overhead.

The paper makes a modest attempt to utilize both primary and secondary membership functions of a GT2FS without increasing computational overhead significantly. The reasoning procedure adopted is neither purely GT2FS nor purely IT2FS, but a mixture of the two, and is referred to as semi-GT2FS reasoning. Here, we use vertical slice representation of GT2FS. Given a measurement point $x = x'$, we consider the contribution of the secondary membership value for each discretized primary membership over the given $x = x'$ line, if the secondary membership value crosses a user-defined threshold, and then compute the geometric mean of the primary and the corresponding (pre-thresholded) secondary membership for all possible discrete primary memberships on the selected $x = x'$ line. Next, we take the maximum and the minimum of the geometric means on the given $x = x'$ line lying inside the footprint of uncertainty (FOU) [20], and redefine these as the revised Upper and Lower membership function values respectively of a given linguistic variable in the antecedent of a type-2 rule. The union of the revised lower (and upper) membership function values at all feasible $x = x'$ reproduces a modified IT2FS corresponding to the given vertical slice GT2FS for the selected linguistic variable *x*. In case we have *n* linguistic variables in the antecedent of a rule, we would have *n* such modified IT2FS, and the inference generation at a given measurement point then is performed following the traditional IT2FS reasoning.

In case *j* (>1) number of rules is fired concurrently, then we take the union of the inferences generated by all the *j* number of rules, and call it the resulting inference. The interval type-2 defuzzification of the resulting inference is computed using Enhanced Karnik-Mendel (EKM) algorithm [21]. Finally, for each rule in the training phase, we provide a possible interval of the resulting defuzzified output of the fired rule to fall in a given class. We classify a color stimulus to fall in class *j*, if the defuzzified output of the fired rule(s) falls in the prescribed interval for the class.

Experiments undertaken confirm that the proposed semi-GT2FS classifier outperforms its competitors with respect to classification accuracy. McNemar's test [53] and Friedman test [54] undertaken also confirm the same results.

The paper is divided into the eight sections. In section II, we provide an overview of color perceptual-ability measurement. Section III introduces the principles used for feature selection by optimization algorithm. In Section IV we propose classifier design using a novel semi-GT2FS classifier. Section V outlines one interesting technique for the perceptual-ability measurement. Experimental details are given in Section VI. Performance analysis and statistical validation are undertaken in Section VII. Conclusions are listed in the Section VIII.

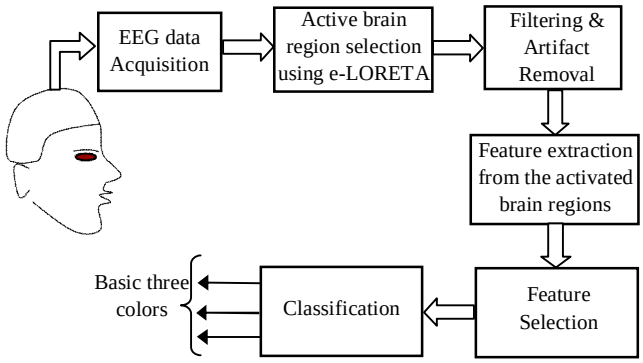

Fig. 1 System overview of color classification using EEG

II. System Overview

Detection of color perceptual-ability of subjects from their brain signals is performed by the following two main steps. First, the brain regions responsible for color-perceptual-ability are identified from the acquired EEG signals using e-LORETA. For convenience, it may be added that e-LORETA employs an inverse mapping to obtain the brain activation patterns from the EEG response, and thereby helps the users in examining the level of activations at different brain regions.

In the second step, electrodes are placed in the brain-regions with high activations following the standard 10-20 electrode placement strategy, and the following sub-steps are performed in sequence to decode the color perceived by the subject.

a) The raw EEG signals are filtered using a Chebyshev type band-pass filter (BPF) with a pass band of (3-10) Hz. The centre of the pass band selection is guided by the location of the peaks in the Fourier spectra and the band-width is determined by the upper and lower 3 dB (decibel) frequencies around the peaks. The Chebyshev filter is selected from its competitors for its good roll-off characteristics around the upper and lower cutoff frequencies. Next, the artifacts lying in the pass-band of the filter are removed by using independent component analysis (ICA) [22].

b)The artifact-free independent components are processed to extract 257 Power-Spectral density (PSD) [23] features by Welch method with a Hamming window of length 64 and 50% overlap between successive windows, and 1278 Daubechies-4 (db-4) discrete wavelet coefficients (DWC) features [24] obtained after third level decomposition.

c) To reduce the computational overhead of the classifier, we reduce the features from 1278+ 257= 1535 to 100 dimensions using a particle swarm optimization (PSO) induced optimal feature selection algorithm.

d) The resulting 100 dimensional features are fed to a classifier for classification of the brain signals into one of 3

basic color classes (red/green/blue). Fig. 1 provides a schematic overview of the complete system.

The most challenging research component of the work lies in the classifier design. As the EEG features suffer from inter-session variations over trials in a day and also across days, we model these variations using type-2 fuzzy sets. Thus we design a type-2 fuzzy classifier to classify the EEG signals into one of three color classes in presence of measurement uncertainty. The proposed classifier is also used to detect the base color from noisy instances of the base color, where the noise is added to the base color by minutely changing the hue, saturation and brightness parameters of the colored noise around the given parameters of the base color.

III. Feature selection using PSO

The number of PSD and wavelet features being large (257+1278= 1535), we like to select a minimum set of features, which are independent of each other. Traditional sequential *forward/backward search algorithms* used for feature selection suffer from the well-known "nesting effect" [25-26], which could be avoided by framing the problem in the settings of optimization. One approach to construct an objective function is to maximize inter-class separating distances and minimize intra-class separating distances, and to optimize the objective function by employing a swarm/evolutionary algorithm.

Let $x_{i,j,k}$ be the i-th feature of the k-th data sample belonging to class j, denoted by G_j. Similar nomenclature applies to $x_{i,j,l}$. Let N be the total number of features, n be the reduced number of features with $n \leq N$. J_1 be a measure of intra-class separation between any two data points $x_{i,j,k}$ and $x_{i,j,l}$ lying in j-th class G_j for j= 1 to R. Similarly, J_2 is a measure of inter-class separation. Evidently, minimization of J_1 and maximization J_2 yields better classification performance.

$$J_1 = \sum_{\forall j}\sum_{\forall i}\sum_{\substack{\forall k,l \in G_j \\ k \neq l}} \left\| x_{i,j,k} - x_{i,j,l} \right\| \quad (1)$$

$$J_2 = \sum_{\forall i}\sum_{\substack{\forall j,\forall j' \in G \\ j \neq j'}}\sum_{\substack{\forall k \in G_j \\ \forall l \in G_{j'}}} \left\| x_{i,j,k} - x_{i,j',l} \right\| \quad (2)$$

$$\text{where } G = \bigcup_{\forall j} G_j \quad (3)$$

One way to minimize J_1 and maximize J_2 is to minimize a new objective function:

$$J_3 = \frac{J_1}{A + J_2}, \quad (4)$$

where, A is a non-zero constant inserted in (4) to avoid division by zero, in case J_2 appears to be zero. The feature selection problem thus boils down to an optimization problem with an aim to select n out of N features for a given value of the parameter A from its user-defined range [45].

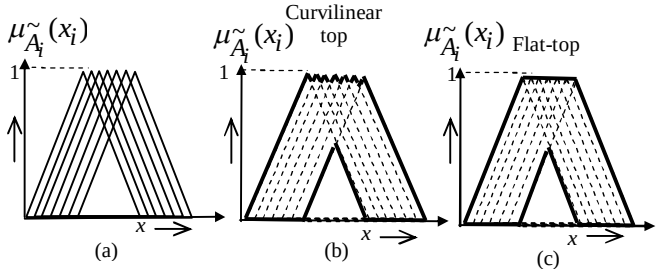

Fig. 2 Construction of IT2FS. (a) Type-1 MFs for seven sessions, (b) Computing union of Type-1 MFs, (c) Flat top approximation of fig. (b)

For optimal choice of the parameter A, we undertake a separate study to attain the maximum classification accuracy for each class of the training data sets (Section VI).

Although any standard meta-heuristic algorithm can be employed to optimize J_3, we, here, select particle swarm optimization (PSO) for its small code, better speed of convergence and our familiarity with this algorithm [27]. The PSO dynamics used has 3 parameters: self-confidence (C_1), swarm confidence (C_2), and inertial weight (ω), which are selected as 2, 2 and 0.729 respectively based on the authors' previous experience [28]. While swarm- and self-confidence parameters are generally assigned as 2 for stability of the PSO dynamics, the choice of inertial weight = 0.729 is determined to balance exploration and exploitation of the particles. Details of PSO are not given here due to space-limitation.

IV. Type-2 Fuzzy Classifier Design

We here propose one IT2FS- and one GT2FS- induced classifier design.

A. IT2FS- induced classifier

IT2FS Construction: Let $\tilde{A}_i$ for i=1 to n be an interval type -2 fuzzy sets (IT2FS) defined as $[\underline{\mu}_{\tilde{A}_i}(x_i), \bar{\mu}_{\tilde{A}_i}(x_i)]$ for a given linguistic variable x_i with $\underline{\mu}_{\tilde{A}_i}(x_i)$ and $\bar{\mu}_{\tilde{A}_i}(x_i)$ as the lower and upper membership function of $\tilde{A}_i$ respectively. To construct $\tilde{A}_i$ we consider both intra-session (comprising 3 trials in a session or day) and inter-session (comprising 7 such sessions in a week) variations in x_i (representing one EEG feature) after stimulating a subject with a specific color stimulus. The mean (M) and standard deviation (σ) of the intra-session variations are computed and a type-1 normal isosceles triangular membership function (MF) is constructed with the centre of the base located at M and its two extremities located at $M \pm 3 \times \sigma$ [29]. An interval type-2 membership function (IT2MF) $\tilde{A}_i$ is constructed by taking the minimum (and maximum) of l (=7) such type-1 MFs (Fig. 2(a)), obtained from experimental instances over l days. The maximum of l constituent type-1 MFs results in a curvilinear top (Fig. 2(b)), which is approximated by a flat top (Fig. 2(c)) by joining the peaks of type-1 MFs [30] to ensure convexity of the resulting MF [31], here used as the

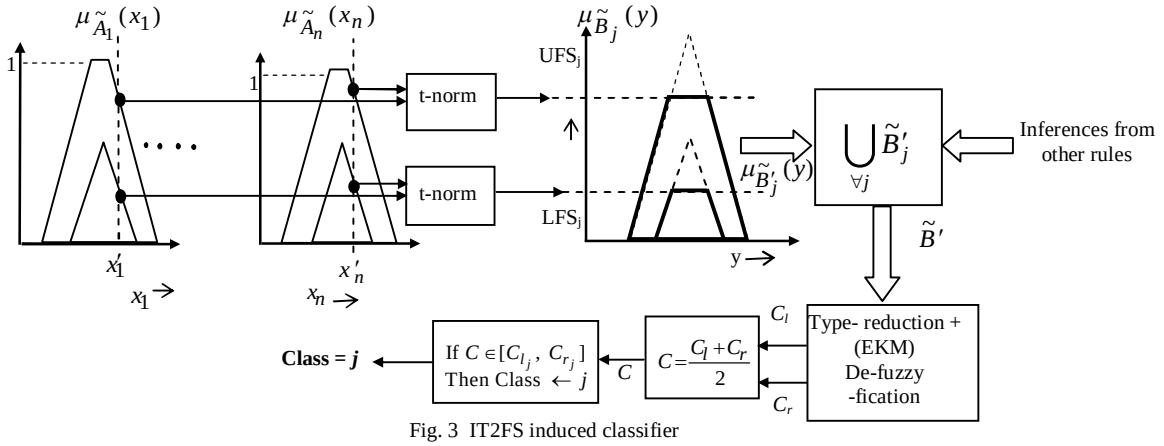

Fig. 3 IT2FS induced classifier

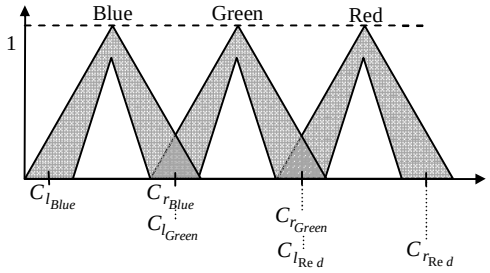

Fig. 4 Consequent IT2 MF for three basic colors (Blue, Green and Red) with initial class centroid positions

UMF of $\tilde{A}_i$. The minimum of the *l* type-1 MFs is defined as the *LMF* of $\tilde{A}_i$.

Classifier Rule: We use the classification rule R_j, given by *If* x_1 *is* $\tilde{A}_1$ *and* x_2 *is* $\tilde{A}_2$ *and ... and* x_n *is* $\tilde{A}_n$, *then* y *is* $\tilde{B}_j$, with class-boundary $[C_{l_j}, C_{r_j}]$, where $\tilde{B}_j$ is a normal isosceles triangular IT2FS with class centroid lying in $[C_{l_j}, C_{r_j}]$. The UMF and the LMF of $\tilde{B}_j$ should have their peaks coincident at the same value of class-centroid axis.

To construct $\tilde{B}_j$ we define a range of class centroid $[C_{l_j}, C_{r_j}]$ for class *j*. While constructing $\tilde{B}_j$, we select the two end points of the base of the triangular UMF as $C_{l_j} - \delta$ and $C_{r_j} + \delta$ for small $\delta > 0$. One choice of δ could be $\delta = (C_{r_j} - C_{l_j})/10$, where the number 10 is selected arbitrarily. The LMF is here constructed with its base-width δ_b% of the base-width of UMF and height δ_h% of the height of the UMF [32]. The peaks of the UMF and the LMF should be coincident over the *x*-axis. The choice of δ_b and δ_h is done using an optimization algorithm to optimize classification accuracy for each class (see Section VI for details).

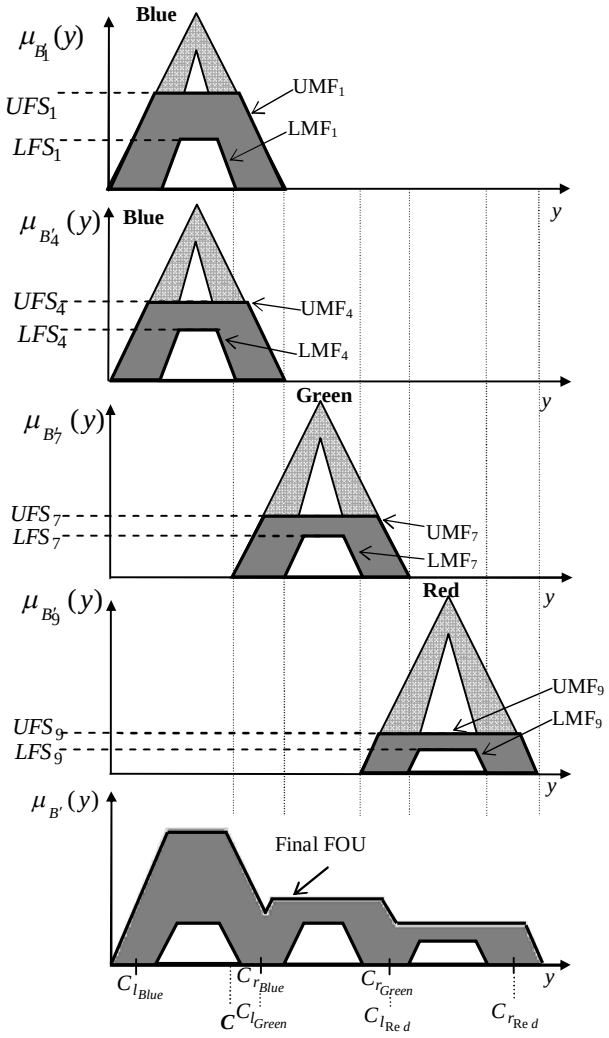

Fig.5 Defuzzified output *C* falls in Blue color class after firing of rules 1, 4, 7 and 9

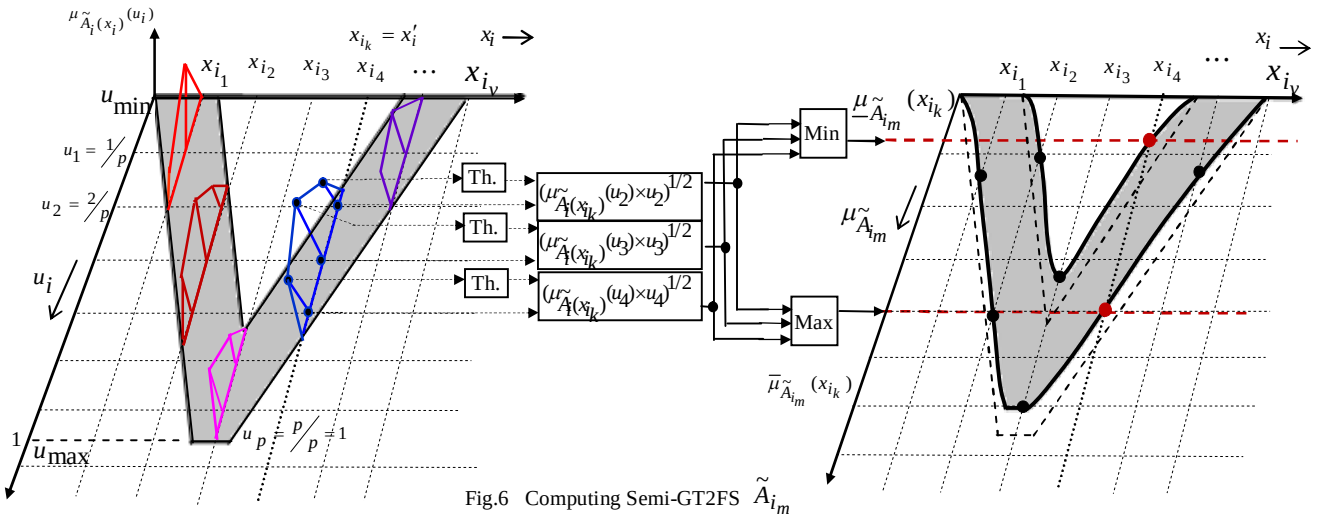

Fig.6 Computing Semi-GT2FS $\tilde{A}_{i_m}$

IT2FS Classifier Design: Suppose, we have *n* measurement points: $x_i = x_i'$ for *i*=1 *to n* features of a brain signal (Fig. 3). We compute upper firing strength (UFS) and lower firing strength (LFS) of rule *j* as

$$UFS_j = T(\bar{\mu}_{\tilde{A}_1}(x_1'), \bar{\mu}_{\tilde{A}_2}(x_2'), ..., \bar{\mu}_{\tilde{A}_n}(x_n')) \quad (5)$$

$$LFS_j = T(\underline{\mu}_{\tilde{A}_1}(x_1'), \underline{\mu}_{\tilde{A}_2}(x_2'), ..., \underline{\mu}_{\tilde{A}_n}(x_n')) \quad (6)$$

where *T* is a cumulative t-norm, defined by $\boldsymbol{T}(\boldsymbol{a}, \boldsymbol{b}, \boldsymbol{c}) = \boldsymbol{t}(\boldsymbol{a}, \boldsymbol{t}(\boldsymbol{b}, \boldsymbol{c})) = \boldsymbol{t}(\boldsymbol{t}(\boldsymbol{a}, \boldsymbol{b}), \boldsymbol{c})$, with t-norm *t* referring to the min (minimum) operator. *T* over an argument of *n* variables can be defined in a similar manner.

Let the consequent MF representation of *j*-th IT2 fuzzy class be $\tilde{B}_j$ .We obtain the IT2 inference $[\underline{\mu}_{\tilde{B}_j'}(y), \bar{\mu}_{\tilde{B}_j'}(y)]$ by the following transformation;

$$\bar{\mu}_{\tilde{B}_j'}(y) = \min(UFS_j, \bar{\mu}_{\tilde{B}_j}(y)) \quad (7)$$

$$\underline{\mu}_{\tilde{B}_j'}(y) = \min(LFS_j, \underline{\mu}_{\tilde{B}_j}(y)) \quad (8)$$

In case multiple rules with same or different class labels in the consequent are fired, we take the union of the IT2 inference to compute the final inference $\tilde{B}'$ by using

$$\tilde{B}' = \bigcup_{\forall j} \tilde{B}_j' = \left[\bigcup_{\forall j} \underline{\tilde{B}'}_j, \bigcup_{\forall j} \bar{\tilde{B}}_j' \right] = [\underline{\tilde{B}'}, \bar{\tilde{B}}']. \quad (9)$$

The $\bigcup$ in (9) represents the union of type-1 fuzzy sets.

Next we type-reduce and defuzzify the IT2 inference $\tilde{B}'$ by Enhanced Karnik-Mendel (EKM) [21] algorithm to obtain C_l and C_r, and obtain centroid *C* as the average of C_l and C_r.

It is indeed important to note that even though there exist overlap in the data points of 2 or more classes, we want the cluster centroids to lie in disjoint contiguous intervals to precisely classify the input data point $[x_1', x_2', ..., x_n']$ into one of *R* classes. Let $[C_{l_j}, C_{r_j}]$ be the possible interval of the *j*-th class centroid, and $[C_{l_{j-1}}, C_{r_{j-1}}]$ and $[C_{l_{j+1}}, C_{r_{j+1}}]$ be the class centroids for neighborhood class $j-1$ and class $j+1$ respectively. Then to maintain contiguous class-boundaries the following conditions should hold for *j*=2 to *R*-1 for *R*-class classification problem:

1) $C_{l_{j-1}} < C_{r_{j-1}}$,

2) $C_{r_{j-1}} = C_{l_j} < C_{r_j}$,

3) $C_{r_j} = C_{l_{j+1}} < C_{r_{j+1}}$.

The choice of class boundaries: $[C_{l_{j-1}}, C_{r_{j-1}}]$ $[C_{l_j}, C_{r_j}]$ and $[C_{l_{j+1}}, C_{r_{j+1}}]$ is obtained optimally with the help of an optimization algorithm introduced in the robustness study in Section VI. Let *C* be a class centroid obtained by EKM algorithm. If *C* lies in $[C_{l_j}, C_{r_j}]$ the inferred class = *j*. Here, we have 3 classes: blue, red and green colors. The consequent IT2MF for 3 basic colors with initial class centroid positions are given in Fig. 4. Computation of centroid from multiple fired rules is illustrated in Fig 5. It is apparent from the figure that the class centroid here lies in $[C_{l_{Blue}}, C_{r_{Blue}}]$, indicating class= blue color.

B. Semi-GT2FS- induced classification

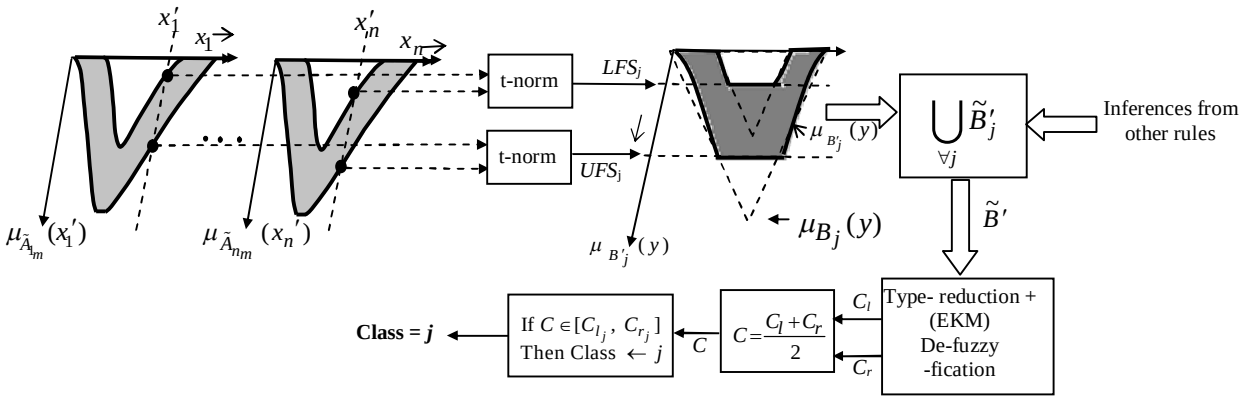

Fig. 7 Inference generation and classification by semi-GT2FS Classifier

Traditional GT2FS based classification yields good classification accuracy at the cost of additional computational overhead [33]. In this paper, we attempt to reduce the computational overhead of GT2FS without losing classification accuracy. This calls for an alternative realization, to transform a GT2FS $\tilde{A}_i$ into an equivalent IT2FS $\tilde{A}_{i_m}$ by considering both primary and secondary MF values of the GT2FS at each value of the linguistic variable [20]. Semi-GT2FS based classifiers offer classification accuracy comparable with its GT2FS-based realization with significantly reduced runtime complexity, comparable to that of IT2FS.

The input of the algorithm is a vertical slice GT2FS, where the vertical slices are placed over distinct values of the linguistic variable $x_i \in X_i = \{x_{i_1}, x_{i_2}, ..., x_{i_v}\}$, where X_i represents the universe of x_i. The algorithm includes 3 steps. In step 1, the entire span of primary membership is partitioned into *p* intervals of equal width. The boundaries of the intervals are represented by *u*-lines: $u_1, u_2, ..., u_p$ (Fig. 6). Step 2 includes 2 basic operations. First, for each x_i-line, $\mu_{\tilde{A}_i(x_{i_k})}(u_i)$-s having values greater than a user-defined small threshold (*th*) of the order of 0.01 are passed on to the next step. This is referred to as *thresholding* (Th. in Fig. 6). The exact value of the threshold (*th*) is obtained by an optimization algorithm, given in Section VI. Next the geometric mean of primary and secondary memberships is computed at each sample point of the vertical slices, where the sample points represent the intersection of *u*-lines with linguistic variable values x_i. The basis of computing geometric mean lies in finding a number greater than the smaller of primary and secondary membership value pairs at the sample points of the vertical slices. In step 3, the largest and the smallest of all possible geometric means computed at the selected sample points over a given x_i-line in each vertical slice are identified, and are treated as contributory points to the modified UMF and LMF on the same x_i-line. The union of the contributory largest (smallest) geometric means corresponding to the vertical slices yields the resulting UMF (LMF) of the modified IT2 membership functions. The pseudo code of the proposed Semi-GT2FS construction algorithm, which is run offline, is given next.

B.1 Pseudo-code for Semi-GT2FS Construction

1. Let $u_{\min} = \underset{x_i \in X_i}{Min}(\underline{\mu}_{\tilde{A}_i}(x_i))$ and $u_{\max} = \underset{x_i \in X_i}{Max}(\bar{\mu}_{\tilde{A}_i}(x_i))$ and then divide $[u_{\min}, u_{\max}]$ into *p* equal intervals of width $\frac{1}{p}$ for a suitable integer *p*, obtained by an optimization algorithm (Section VI). In Fig. 6, u_i is assigned a value $\frac{z}{p}$, for *z* = 1 to *p*, where $u_{\min} < u_1 < u_2 < ... < u_p \le u_{\max}$.

2. For integer *i* = 1 to *p*, if $u_i \ge th$, where *th* is a user-defined threshold, determined by an optimization algorithm (Section VI), then compute the type-reduce IT2FS at $x_i = x_i' = x_{i_k}$, say, given by

$$\underline{\mu}_{\tilde{A}_{i_m}}(x_{i_k}) = \min_{\forall i}\{(u_i \times \mu_{\tilde{A}_i(x_{i_k})}(u_i))^{1/2}\} \quad (10)$$

$$= \min_{z=1}^{p}\{(\frac{z}{p} \times \mu_{\tilde{A}_i(x_{i_k})}(\frac{z}{p}))^{1/2}\} \quad (11)$$

and

$$\bar{\mu}_{\tilde{A}_{i_m}}(x_{i_k}) = \max_{\forall i}\{(u_i \times \mu_{\tilde{A}_i(x_{i_k})}(u_i))^{1/2}\} \quad (12)$$

$$= \max_{z=1}^{p}\{(\frac{z}{p} \times \mu_{\tilde{A}_i(x_{i_k})}(\frac{z}{p}))^{1/2}\} \quad (13)$$

where the modified IT2 MF $\mu_{\tilde{A}_{i_m}}(x_{i_k})$ satisfies the inequality: $\underline{\mu}_{\tilde{A}_{i_m}}(x_{i_k}) \le \mu_{\tilde{A}_{i_m}}(x_{i_k}) \le \bar{\mu}_{\tilde{A}_{i_m}}(x_{i_k})$ for all integer *k* in [1, *v*].

3. To compute modified UMF and LMF, the following operations are undertaken,

$$\underline{\mu}_{\tilde{A}_{i_m}}(x_i) = \bigcup_{\forall k} \underline{\mu}_{\tilde{A}_i}(x_{i_k}), \quad (14)$$

and $$\bar{\mu}_{\tilde{A}_{i_m}}(x_i) = \bigcup_{\forall k} \bar{\mu}_{\tilde{A}_i}(x_{i_k}) \quad (15)$$

thereby producing the *Footprint of Uncertainty* (FOU) of $[\underline{\mu}_{\tilde{A}_{im}}(x_i), \overline{\mu}_{\tilde{A}_{im}}(x_i)]$. This is repeated for all fuzzy sets $\tilde{A}_i$, i = 1 to n.

B.2 Classification with Semi-GT2FS Antecedent MFs

Let us consider a GT2FS rule of the same format like rule R_j where $\tilde{A}_i$ for i=1 to n are GT2FS and $\tilde{B}$ is a triangular IT2FS, representing the MF of class label j with the peak of its UMF and LMF at the center of its base. Let $x_1 = x_1', x_2 = x_2', ..., x_n = x_n'$ be an n-dimensional measurement point. The following steps are executed online for the present classification problem.

1.Obtain $\mu_{\tilde{A}_{1m}}(x_1), \mu_{\tilde{A}_{2m}}(x_2), ..., \mu_{\tilde{A}_{nm}}(x_n)$, at the measurement point: $x_1 = x_1', x_2 = x_2', .., x_n = x_n'$ respectively. Compute the t-norms, given by (16) and (17) to evaluate the Lower and the Upper Firing Strengths: UFS_j and LFS_j for the rule j.

$$UFS_j = T(\overline{\mu}_{\tilde{A}_{1m}}(x_1'), \overline{\mu}_{\tilde{A}_{2m}}(x_2'), ..., \overline{\mu}_{\tilde{A}_{nm}}(x_n')) \quad (16)$$

$$LFS_j = T(\underline{\mu}_{\tilde{A}_{1m}}(x_1'), \underline{\mu}_{\tilde{A}_{2m}}(x_2'), ..., \underline{\mu}_{\tilde{A}_{nm}}(x_n')) \quad (17)$$

where T is a cumulative t-norm.

2. Compute:

$$\overline{\mu}_{\tilde{B}_j'}(y) = \min(UFS_j, \overline{\mu}_{\tilde{B}_j}(y)) \quad (18)$$

$$\underline{\mu}_{\tilde{B}_j'}(y) = \min(LFS_j, \underline{\mu}_{\tilde{B}_j}(y)). \quad (19)$$

3. In case multiple rules with same or different class labels in the consequent are fired, we take the union of the IT2 inference $\tilde{B}_j'$ to compute the final inference $\tilde{B}'$ by using

$$\tilde{B}' = \bigcup_{\forall j} \tilde{B}_j' = \left[\bigcup_{\forall j} \underline{\tilde{B}}_j', \bigcup_{\forall j} \overline{\tilde{B}}_j'\right] = [\underline{\tilde{B}}', \overline{\tilde{B}}']. \quad (20)$$

The $\bigcup$ in (20) represents the union of type-1 fuzzy sets.

4. Use Enhanced Karnik-Mendel (EKM) de-fuzzification [21] on $[\underline{\tilde{B}}', \overline{\tilde{B}}']$ to obtain C_l and C_r, the left and right end point centroids respectively.

5. For each rule j we repeat step 1 through 4 to obtain C_{l_j}, C_{r_j} for j = 1 to R rule, we then search the centroid C at the consequent in $[C_{l_j}, C_{r_j}]$ for all j. If $C_{l_j} < C < C_{r_j}$ then ***class = j.*** This is illustrated in Fig. 7.

It is important to note that for classification in real time, we simply need to evaluate part of the semi-GT2FS corresponding to one vertical plane of the antecedent GT2FS at the given measurement point. Then we need to perform the classification steps 1 to 5 in real time.

Time-Complexity: The proposed semi-GT2FS classifier has the worst-case time-complexity of $O(p+2n)$ where n denotes the number of linguistic variables in the antecedent and p denotes the number of discretizations along the $\mu_{\tilde{A}_i}(x_i)$ axis. Note that traditional z-slice based classifiers [34] have the worst-case complexity of $O(p \times v \times I)$ where v is the number the number of vertical slices along the x_i axis, and I is the number of z-slices in each antecedent GT2FS. Further, traditional vertical slice based classifier [17] have the worst-case time-complexity of $O(p^n)$. So, complexity-wise the proposed GT2FS classifier outperforms existing vertical-slice and z-slice based classifiers.

C. Secondary membership evaluation

Let $[\underline{\mu}_{\tilde{A}_i}(x_i), \overline{\mu}_{\tilde{A}_i}(x_i)]$ be a given IT2FS, we need to determine the secondary MF $\mu_{\tilde{A}_i(x_i)}(u_i)$ at $x_i = x_i'$ say. The following assumption are considered to maintain convexity of secondary MF on a vertical plane at $x_i = x_i'$.

1. The secondary MF $\mu_{\tilde{A}_i(x_i')}(u_i)$ would have a small non-negative value at $u_i = u_p$ and $u_i = u_q$, the extremities of u_i over the $x_i = x_i'$ line. This is reasonable as the certainty of primary membership is minimum at the extremities of the FOU for any given value of the linguistic variable $x_i = x_i'$.

2. The secondary MF $\mu_{\tilde{A}_i(x_i')}(u_i)$ would have the peak at the centre of the FOU $u_i = u_{mid} = (u_p + u_q)/2$ on the given $x_i = x_i'$ line.

3. For a given $x_i = x_i'$, if $u_i \in [u_p, u_q]$,

$$\mu_{\tilde{A}_i(x_i')}(u_i) = \max[\mu_{\tilde{A}_i(x_i')}(u_{mid}).\exp(-|u_{mid} - u_i|), \max(\mu_{\tilde{A}_i(x_i')}(u_p), \mu_{\tilde{A}_i(x_i')}(u_q))] \quad (21)$$

The justification of the last formula is apparent as the secondary MF $\mu_{\tilde{A}_i(x_i')}(u_i)$ at $x_i = x_i'$, decreases exponentially as u_i is away from u_{mid}. However, the secondary membership of u_i should be greater than the secondary membership of u_p and u_q on the given $x_i = x_i'$ line.

It is important to mention here that we need to select class boundaries: C_{l_j} and C_{r_j} of each rule j with an aim to maximize the classification accuracy for each class. This is done by using a DE algorithm at the validation stage of the system with training instances labeled with class information. In our realization, we optimized C_{l_j} and C_{r_j} of the IT2 class j as indicated in the consequent part of rule j for all j.

V. Color Perceptual-Ability Measurement

Color perceptual-ability refers to the power of discriminating color, particularly in presence of noisy color instances. For example, a red color stimulus, when induced with a non-red

color of relatively lower brightness, the latter is treated as a color noise to the former. One simple approach of injecting noise to a color stimulus is to adjust the hue, saturation and/or brightness. The hue of redness, for example, is controlled by injecting other two basic colors (blue and green) of desired proportions in the R-G-B color space. Brightness of red color is controlled by adding white color of desired proportion to the red stimulus. Saturation refers to the degree of the color content [35]. For instance, a red stimulus with low saturation turns into a gray stimulus, while the same red stimulus with maximum saturation retains the pure (100%) redness of the stimulus. We employed the above three parameters to represent the color noise.

The motivation of the present study is to determine the color perceptual-ability of subjects from the electrical response of the brain due to color stimuli. Although different modalities of brain imaging, including electroencephalography, functional Near Infrared spectroscopy (f-NIRs) and functional magnetic resonance imaging (f-MRI) are available in the literature, we prefer EEG over others for its excellent temporal response, non-invasiveness and portability.

The following definitions would be useful to understand the rest of the paper.

Let $\bar{x}_{1,j}, \bar{x}_{2,j}, \ldots\ldots, \bar{x}_{n,j}$ be the average value of the features for class *j*. the averaging is done on the training data set corresponding to each feature under class *j*. for instance,

$$\bar{x}_{i,j} = \frac{1}{F}\sum_{k=1}^{F} x_{i,j,k} \tag{22}$$

where,

$x_{i,j,k}$ denotes the *k*-th instance of the feature *i* under class *j*.

F = No. of instances of *j*. Let $X_{i,l}$ be the *l*-th instance of the *i*-th feature for the test data.

We construct a distance between $\bar{x}_{i,j}$ and $X_{i,l}$ for all features *i* = 1 to *n*. We call it $d_{j,l}$ where

$$d_{j,l} = \left[\sum_{i=1}^{n} (\bar{x}_{i,j} - X_{i,l})^2\right]^{1/2} \tag{23}$$

Now, for $j = 1 \text{ to } R$ classes, we obtain $d_{j,l}$. Suppose, $d_{j,l} \le d_{j',l}. \forall j'$, we declare the *class* = *j* as the class of the *l*-th instances of the test data. We define the recognition probability of *l*-th test data given by,

$$pr_l = 1 - \frac{d_{j,l}}{\sum_{j'=1}^{R} d_{j',l}}. \tag{24}$$

Now, for *l* = 1 to *Q* instances for unknown test data, we compute Average Recognition Probability

$$ARP = \frac{1}{Q}\sum_{l=1}^{Q} pr_l \,. \tag{25}$$

Now, for *S* subjects we compute the average recognition probability for all subjects and sort it in descending order. The index of the sorted element indicates the value of the subject in the color recognition ability.

Discrimination ability: Suppose, by recognition-ability, we have the *l*-th instance $[X_{1,l}, X_{2,l}, \ldots, X_{n,l}]$ falling in class *j*. Then we distort the input stimulus by changing its hue, saturation and brightness independently until the class change is observed. The maximal distortion of the stimulus for which its recognition is acceptable is a measure of discrimination-ability of the subject in presence of color noise. Let $\bar{x}_{1,j}, \bar{x}_{2,j}, \ldots\ldots, \bar{x}_{n,j}$ be the mean values of *n* selected feature for class *j*. Suppose, an unknown color (without noise) falls in class $j \in 1, 2, \ldots, R$. We then change hue, saturation and brightness around their center values for which the stimulus is still classified as *j*. Let the changes be $[h^* - \Delta h, h^* + \Delta h]$, $[s^* - \Delta s, s^* + \Delta s]$ and $[b^* - \Delta b, b^* + \Delta b]$ where Δh, Δs and Δb are the changes of hue, saturation and value with respect to their center value h^*, s^* and b^* respectively for which the stimulus is recognized as class *j*. We repeat it for all unknown test data points on all subjects. A subject showing the largest change in the product-sum, called Recognition-Tolerance,

$$RT = \sum_{\forall stimulus} \Delta h \times \Delta s \times \Delta b \tag{26}$$

for all the stimuli is recognized to be most robust. We need to rank the people in descending order of their $ARP \times RT$.

VI. Experiments And Results

This section deals with four distinct experiments: 1) detection of active brain regions responsible for the recognition of the primary colors, 2) frequency band selection for artifacts removal, 3) selection of the EEG features from the activated brain regions for the classification of three primary colors, and 4) Optimal parameter setting of the feature selection and classifier unit. Here we give a brief overview of the EEG acquisition machine, the experimental set-up along with the details of stimuli preparation and presentation.

A. EEG data acquisition and Experimental set-up

Experiments are conducted using a standard 21 channels Nihon Kohden EEG data acquisition system having a sampling rate of 500 Hz to capture the EEG signals from the scalp of the subjects with the help of Ag/AgCl electrodes [36]. The electrodes are placed at the Fp_1, Fp_2, F_3, F_4, F_7, F_8, C_3, C_4, P_3, P_4, O_1, O_2, T_3, T_4, T_5, T_6, F_z, C_z and P_z locations according to the international 10/20 system for EEG recording [37]. The Fp_z electrode is used as the ground and two earlobe electrodes A_1 and A_2 are used as the references for the right- and the left-side electrodes respectively [38].

The experiment has been performed on 3 colored and noisy colored databases, namely Jadavpur university database (JUDB) [39], South-West Bengal database (SWBDB) [40], North-Indian Database (NIDB) [41], developed by Artificial Intelligence Laboratory of

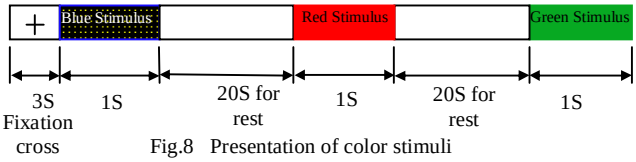

Fig.8 Presentation of color stimuli

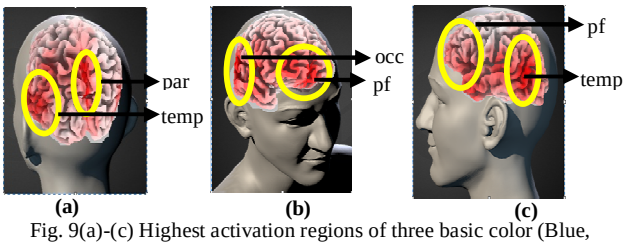

Fig. 9(a)-(c) Highest activation regions of three basic color (Blue, Red and Green)

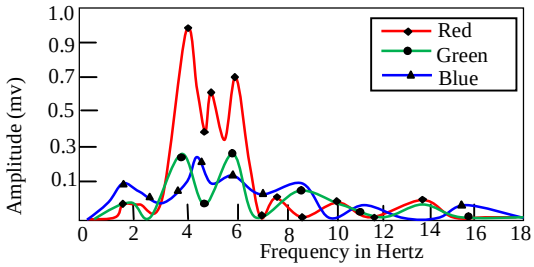

Fig. 10 Selection of frequency bands (3-10) Hz for color light from Occipital region (O_2 electrode)

TABLE I
ACTIVATION OF SCALP MAPS FOR THREE COLOR STIMULI AT DIFFERENT FREQUENCY BANDS

Frequency Bands	Blue color	Red color	Green color
Scalp map at upper theta and lower alpha bands	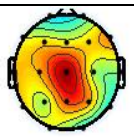 4.2Hz	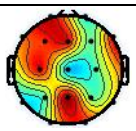 4 Hz	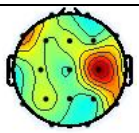 3.9 Hz

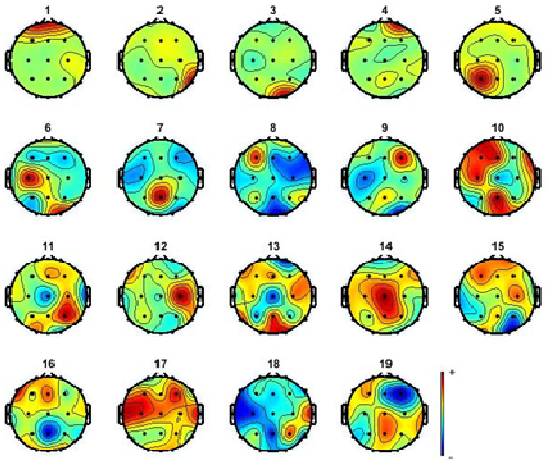

Fig. 11 Scalp maps for blue color stimulus using ICA

Jadavpur University for color perception experiments on different regional groups of people of India. Unfortunately, no other database was found in the internet to study the relative performance of the proposed algorithms on databases prepared by other research groups. Each of the above databases includes perceived EEG response of 30 healthy subjects (with normal eyesight) to color stimuli, for people in the age-group of 22-30 years. The JUDB and SWBDB comprise data of 18 men and 12 women, while NIDB includes data of 16 men and 14 women. While preparing the databases, the volunteers are advised to sit on a comfortable chair in the resting condition without movement to eliminate the possibility of contamination by movement-related artifacts. Visual stimulus in the wavelength (700nm ± 20nm), (530nm ± 20nm) and (470nm ± 20nm) respectively for red, green and blue colors are generated by a remote controlled 15W RGB flood light with 110-220V power supply. The room was intentionally kept dark to avoid unwanted incidence of any other light on the subject's eyes. The intensity of each colored light is increased to a maximum limit within the pre-tested tolerance level of the subjects.

In all the 3 databases, each subject is exposed to one of three colored lights continuously for one second. To avoid the residual effect of the previous colored light, a time-gap of 20 second is maintained between two successive presentations of color stimuli. Each of the 3 databases includes 7 days' data of each subject with 3 trials/color/day. Thus for 30 people, the databases includes 30 × 7 × 3 × 3= 1890 data. The sequence of presentation of the colored light was randomly selected in each trial from the list: red, green and blue. Fig. 8 illustrates one sequence of color stimuli. The results/graphs presented in the experiments below are demonstrated with JUDB only for space restriction.

B. Experiment 1: Selection of active brain region using e-LORETA

In this experiment, we evaluate the electrical activity of the intra-cortical distribution obtained from the EEG data (of JUDB) using e-LORETA software [42]. To determine the highly active brain regions for three different color stimuli, we use linear inverse solution technique. The total experimental duration of 1000ms (=1 sec) color stimulation is divided into 640 time-frames of 1.562 ms under the e-LORETA framework. It is apparent from the activation values of different time frames (Fig. 9 (a-c)) that the parietal lobe is highly activated for the blue color, whereas the pre-frontal and temporal lobe are highly activated for the red and the green colors respectively at early stage of the brain activation. High activation in selected brain regions reveal that the blue color is expected to influence smart planning, whereas the red color helps in instantaneous decision-making and the green color helps in memory activation and recall. Further experiments with f-MRI device can confirm these results.

C. Experiment 2: Filtering and Artifact Removal

This section aims at evaluating an appropriate filter to determine the desired characteristics of color stimulus. To select the exact frequency band, we need to take Fourier transform of the EEG signals. The highest amplitude of the Fourier spectra for three basic colors (red, green and blue) lies between 3 to 10 Hz. Here, we take Chebyshev filter of order 10 as an active digital band pass filter. To select the pass band of the Chebyshev filter for three different color stimuli, we require the center-frequency [43] of the bands

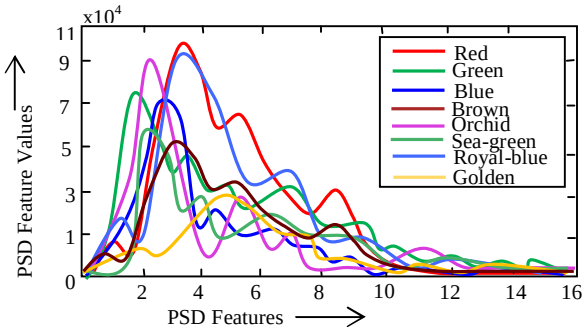

Fig.12 PSD Features extracted from O_2 electrode for eight inter class color stimuli

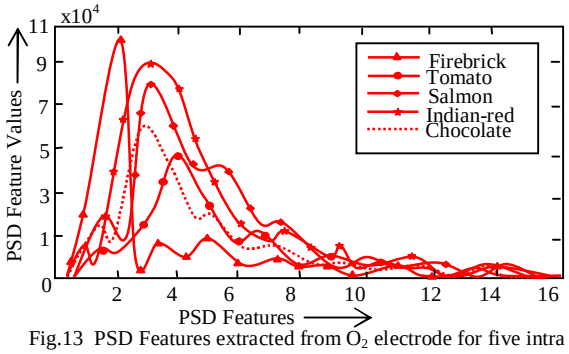

Fig.13 PSD Features extracted from O_2 electrode for five intra class color stimuli

and scalp maps for three basic colors, as given in Table-I.

The frequency response of the basic colors from the Occipital region is given in Fig. 10. To isolate the artifacts and Event Related Potential (ERP) signals from the recoded EEG signals, we use Independent Component analysis (ICA). For color recognition task, we take ICA of 19 individual electrodes. The scalp map of blue color stimulus obtained from 19 ICA components are shown in Fig. 11. The figure includes circular red contour of the independent components 5, 6, 7, 8, 9, 12, 14 due to the activation of the corresponding brain regions. The remaining components are ignored as those are activated by artifacts possibly due to eye-blinking.

D. Experiment 3: Extraction of EEG features from active brain regions

In this experiment, we undertake classification of color stimuli within and across color classes. To extract important EEG features, we consider all possible time-, frequency-, and time-frequency co-related features like Power Spectral Density (PSD), Discrete Wavelet Transform (DWT). Here, we realize eight different color stimuli for thirty subjects with 21 trials each. For each color class in a trial of an experimental subject, we have 257 PSD features and 1278 wavelet features. Fig. 12 and 13 represent PSD features of the brain response recorded from Occipital region for 8 different color stimuli, referred to as inter-class color variation, and five selected intra-class color stimuli, generated by varying hue, saturation and brightness of a basic color (here red) from the same brain region. It is apparent from Fig. 13 that the 4th and the 5th PSD features have sufficient information to segregate all the 5 noisy (intra-) class color stimuli, with red as the base color.

E. Experiment 4: Robustness Study by Optimal parameter setting

One approach to ensure robustness of the proposed IT2FS and GT2FS classifier algorithms is to fix the optimal parameter set of the classifiers with respect to a given criterion. Here, we need to select the parameters of the classifiers with an aim to maximize the classification accuracy (CA) for each class. Let

$\psi = \{\delta_b, \delta_h, C_{l_{Blue}}, C_{r_{Blue}}, C_{l_{Green}}, C_{r_{Green}}, C_{l_{\mathrm{Red}}}, C_{r_{\mathrm{Red}}}\}$ and

$\psi' = \{\delta_b, \delta_h, p, th, C_{l_{Blue}}, C_{r_{Blue}}, C_{l_{Green}}, C_{r_{Green}}, C_{l_{\mathrm{Red}}}, C_{r_{\mathrm{Red}}}\}$

be the parameter sets of the IT2FS and the GT2FS classifiers respectively, and $J = \sum_{j=1}^{R} CA_j$ be the selected objective function to be optimized. Here, CA_j denotes the classification accuracy of the *j*-th class with respect to the given training instances. Fig 14 (a) provides a schematic overview for online computation of classification accuracy of the training instance data for class *j*. Here, the actual class (*AC*) and the predicted class (*PC*) produced by the classifier are compared for all data points falling in class *j*. A variable *match-score* is used to count the number of times *PC* =*AC* for $|CL_j|$ number of data-points in class *j*. After the algorithm exits the loop (Fig. 14), the percentage classification accuracy (PCA) for class *j* is evaluated by $match-score/|CL_j| \times 100$. The process of online computation of PCA is repeated for *j* =1 to *R* classes.

In Fig. 14(b), provides a scheme for optimal selection of classifier parameters ψ_{opt} for IT2FS (ψ'_{opt} for GT2FS classifiers, not shown) and parameter *A* used for feature selection. The parameter *A* is optimized by a grid-search algorithm [53], where the ψ_{opt} (or ψ'_{opt}) is obtained by an Evolutionary Optimization algorithm. Both the grid-search and Evolutionary Optimization algorithm have a common performance meaning index, $J = \sum_{j=1}^{R} CA_j$. Here, we need to maximize *J*, and thus obtain optimal parameters ψ_{opt} (or ψ'_{opt}) and A_{opt}. The grid-search algorithm selects *A* in $[A_{\min}, A_{\max}]$ in each iteration and passes on the value of *A* to feature selection algorithm, realized with PSO. The feature selection algorithm utilizes the selected value of *A* and feeds the selected feature of the classifier to determine classification accuracy with respect to the labeled training instances. The results of classification accuracy of each class are used to obtain the performance metric *J*.

The Differential Evolution (DE) algorithm is used to compute optimal parameter set ψ_{opt} for IT2FS (and ψ'_{opt} for GT2FS) classifiers. The evolved parameter set ψ of the classifier is transferred back to the classifier after each evolutionary step, till the DE converges. Although any traditional or meta-heuristic algorithm can be employed

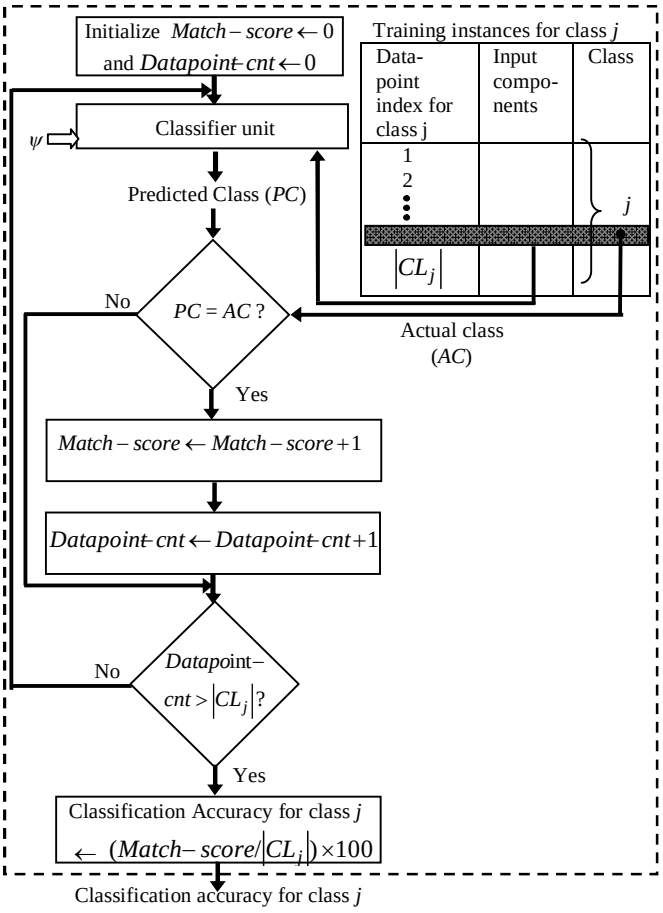

Fig.14 (a) Computation of classification accuracy for class *j* in the training phase

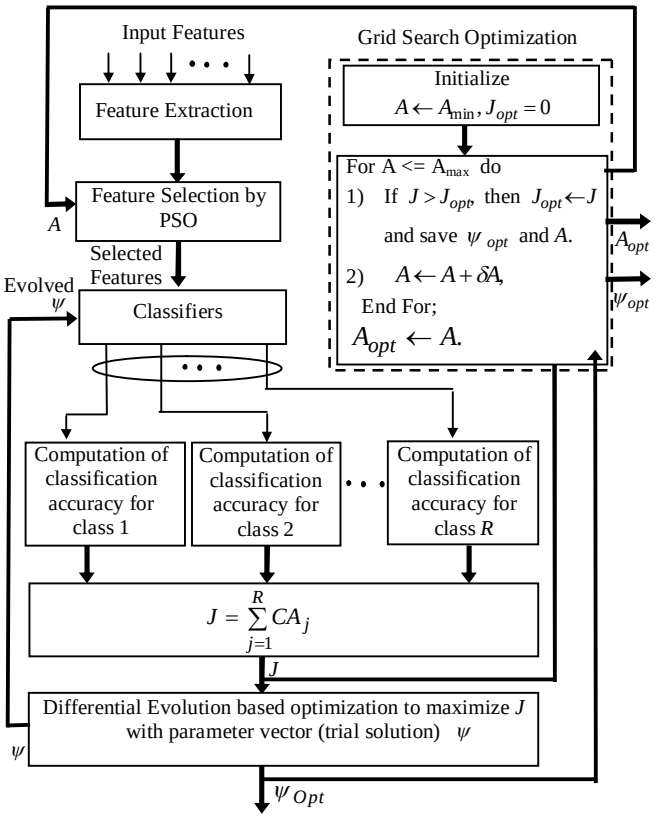

Fig.14 (b) Computation of DE based optimal parameter set ψ_{Opt} to optimize *J*

to optimize the objective function, DE is used for the present application for its high speed, fewer parameters, good computational accuracy, and the authors' familiarity with the algorithm [44-45] for a long time. DE is used here instead of PSO to avoid confusion of the readers in using the same algorithm for two different optimization tasks. The DE/rand/1/bin version is used for the present application with scale factor $F = 0.7$ and crossover with crossover rate $C_r = 0.8$. After the DE converges, the parameter vector ψ_{opt} (ψ'_{opt}) with the best measure of fitness *J* for a selected *A* in $[A_{\min}, A_{\max}]$ are transferred to the Grid Search algorithm for optimal selection of *A*.

The Grid Search algorithm [46] is initialized with $A = A_{\min}$ and $J = J_{opt} = 0$. The algorithm checks whether the *J* obtained for a given *A* is less than J_{opt}. If yes, J_{opt} is redefined as the recently computed *J*. The grid search algorithm also increments *A* by δA, where $\delta A = (A_{\max} - A_{\min})/H$, where *H* is a user-defined integer, selected as 100. The algorithm thus keeps track of the optimal *J* and the optimal classifier parameters ψ_{opt} (ψ'_{opt}) and A_{opt}, where A_{opt} is the optimal value of *A* for $J = J_{opt}$ for all *A* in $[A_{\min}, A_{\max}]$.

The optimal overall system parameters obtained for IT2FS-based classification are: $A = 0.052$, $\delta_b = 80.8\%$, $\delta_h = 74.2\%$, $C_{l_{Blue}} = 5.26$, $C_{r_{Blue}} = C_{l_{Green}} = 28.56$, $C_{r_{Green}} = C_{l_{Red}} = 65.82$, and $C_{r_{Red}} = 95.74$.

The optimal values of the system parameters obtained for Semi-GT2FS classification are listed below:

$A = 0.054$, $\delta_b = 80.2\%$, $\delta_h = 73.8\%$, $p = 12$, $th = 0.02$, $C_{l_{Blue}} = 8.26$, $C_{r_{Blue}} = C_{l_{Green}} = 28.31$, $C_{r_{Green}} = C_{l_{Red}} = 67.39$, and $C_{r_{Red}} = 97.61$.

F. Effect of parametric drift from their optimal settings

The parameter *A* controls the list of selected features and thus is indirectly responsible for selecting the set of rules to fire based on the instantiation of the rules by the selected features. Because of changes in the set of fired rules, the overall inference (obtained by taking union of the inferences of the fired rules) change, causing a change in the Type-2 centroid. Additionally, because of the drift in class boundaries ($C_{l_{Blue}}$, $C_{r_{Blue}} = C_{l_{Green}}$, $C_{r_{Green}} = C_{l_{Red}}$, and $C_{r_{Red}}$) from their optimal values, the computed Type-2 centroid of the final inference falls within the bounds of different classes, resulting in misclassification.

Fig. 15 provides a comparative analysis of the structure and the centroid of the final FOUs due to drift in the set of classifier parameters ψ from their optimal settings. Fig. 15(a) provides the FOU with the optimal parameter setting. In Fig. 15(b), all the tunable parameters excluding parameter

A have been changed. It is observed from the above figures that the structure of the final FOU changes even with same set of fired rules due to optimal setting of *A* in both Fig. 15(a) and (b). In Fig. 15 (c), the effect of variation of all parameters listed in ψ including *A* is shown. It is apparent from 15(a) and (c) that the final FOU changed significantly, and the computed centroid falls in a false class due to misclassification.

Similar experiment is performed for semi-GT2FS classifier. In case of semi-GT2FS, the FOU of the modified antecedent MFs undergo changes due to drift in the set of classifier parameters ψ' and *A* from their optimal settings. This is illustrated in Fig. 16(a-d). It is apparent from the figure that a deviation in the classifier parameters and *A* from their optimal settings causes an increase in the area under the FOU of the antecedent semi-GT2FS MFs. This change in antecedent MFs effectively results in an increase in the area of the final inferential FOU with respect to the same obtained for optimal parameter settings. The centroid of the final FOU shifts from their original values, computed with optimal setting of classifier parameters and *A*. The phenomena being similar with that of IT2FS are not graphically illustrated due to space limitation.

G. Experiment 5: Sensitivity Analysis

In this experiment, we undertake sensitivity analysis from the resulting drift in classification accuracy for deviation in classifier parameters from their optimum values. In this experiment, one of the 7 parameters: A, δ_b, δ_h, $C_{l_{Blue}}$, $C_{r_{Blue}} = C_{l_{Green}}$, $C_{r_{Green}} = C_{l_{\mathrm{Red}}}$, and $C_{r_{\mathrm{Red}}}$ for the IT2FS classifier is off-tuned from its optimum value, and classification accuracy is evaluated with one off-tuned and optimal setting of the remaining 6 parameters values. Fig. 17 (a)- (g) provide the plots of classification accuracy versus selected off-tuned parameter. It is found from the plots that the peak in classification accuracy occurs at its optimum value. Once the parameter is drifted slightly from its optimal value, the classification accuracy falls off by a large margin. Similar experiment is performed for semi-GT2FS classifier with 9 optimal parameters: A, δ_b, δ_h, p, th, $C_{l_{Blue}}$, $C_{r_{Blue}} = C_{l_{Green}}$, $C_{r_{Green}} = C_{l_{\mathrm{Red}}}$, and $C_{r_{\mathrm{Red}}}$ with plots of classification accuracy versus drift in individual parameters from its optimal value

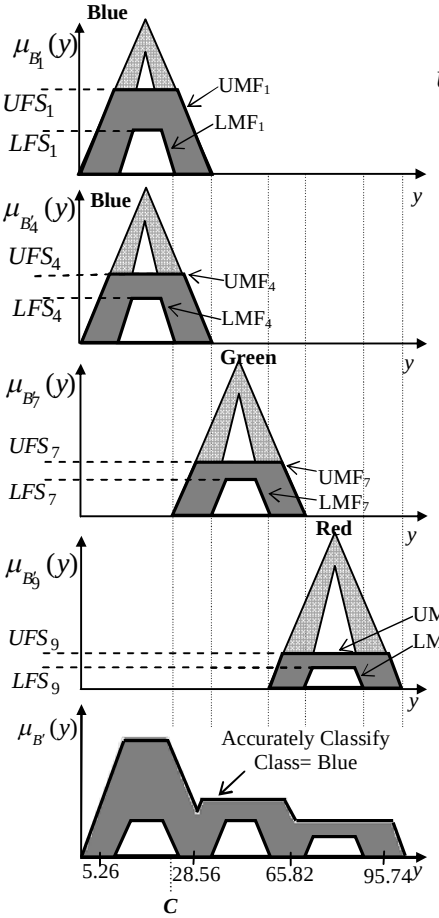

Fig.15(a) IT2FS FOU for optimal setting of classifier parameters: A = 0.052, δ_b = 80.8%, δ_h = 74.2%, $C_{l_{Blue}}$ = 5.26, $C_{r_{Blue}}$ = $C_{l_{Green}}$ =28.56, $C_{r_{Green}} = C_{l_{\mathrm{Red}}}$ = 65.82, and $C_{r_{\mathrm{Red}}}$ = 95.74

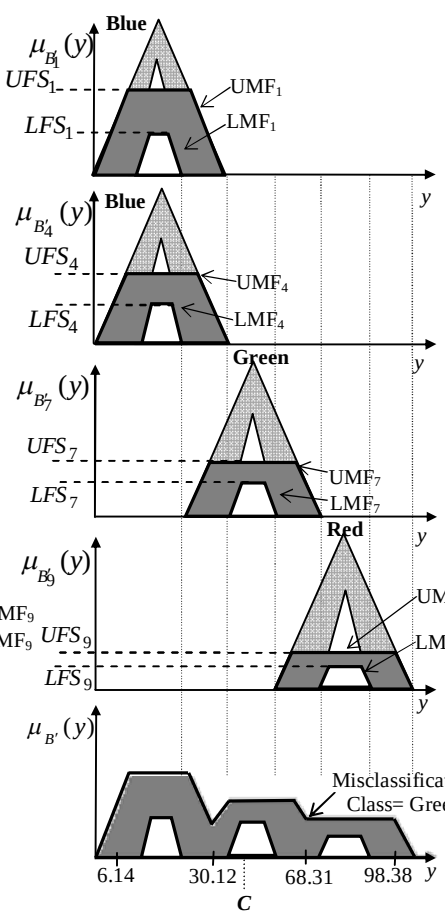

Fig.15(b) Change in IT2FS FOU for drift in classifier parameters excluding *A* from their optimal values to: A = 0.052, δ_b = **82.5%,** δ_h **=79.7%,** $C_{l_{Blue}}$ = **6.14,** $C_{r_{Blue}} = C_{l_{Green}}$ = **30.12,** $C_{r_{Green}}$ = $C_{l_{\mathrm{Red}}}$ **= 68.31,** and $C_{r_{\mathrm{Red}}}$ **= 98.38**

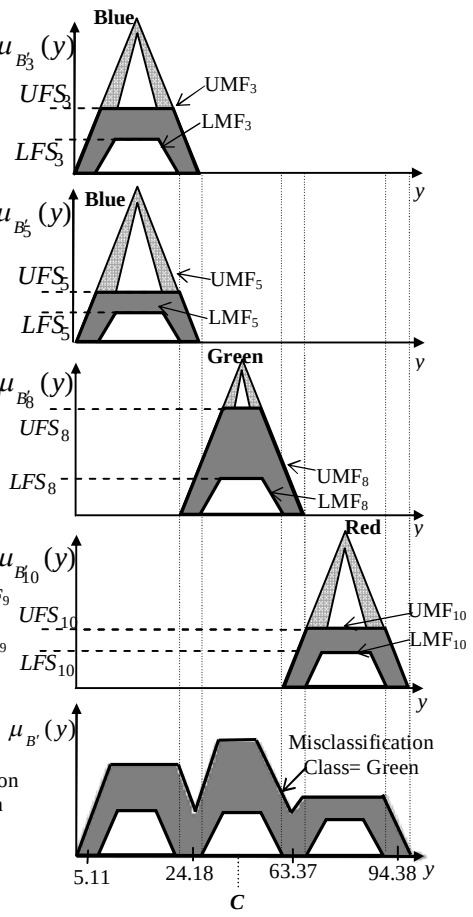

Fig.15(c) Change in IT2FS FOU for drift in classifier parameters including *A* from their optimal values to: A = **0.066,** δ_b **=74.2%,** δ_h **=65.5%,** $C_{l_{Blue}}$ = **5.11,** $C_{r_{Blue}} = C_{l_{Green}}$ **=24.18,** $C_{r_{Green}} = C_{l_{\mathrm{Red}}}$ **=63.37, and** $C_{r_{\mathrm{Red}}}$ **= 94.38**

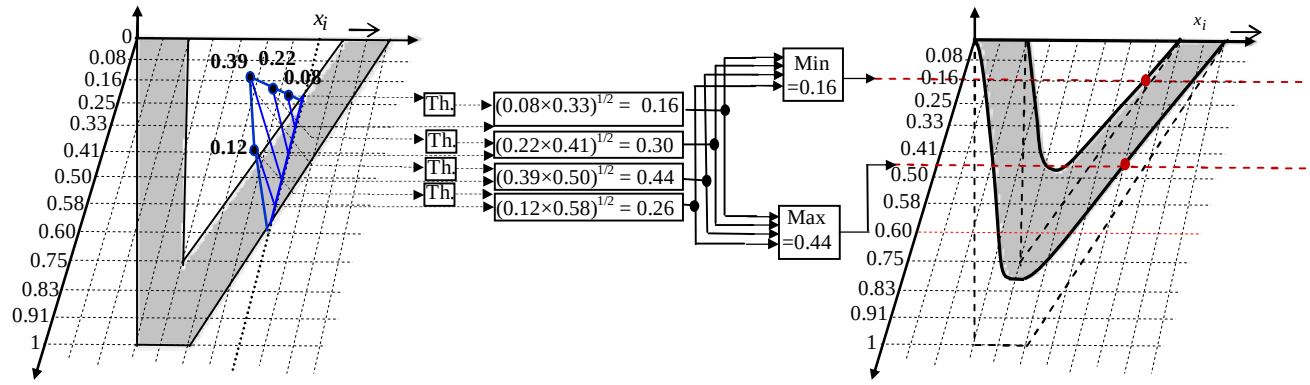

Fig.16 (a) Modified semi-GT2FS FOU for the setting of optimal parameter: $A=0.054$ $\delta_b = 80.2$, $\delta_h = 73.8$, $p=12$, $th=0.02$, $C_{l_{Blue}} = 8.26$, $C_{r_{Blue}} = C_{l_{Green}} = 28.31$, $C_{r_{Green}} = C_{l_{Red}} = 67.39$, $C_{r_{Red}} = 97.61$

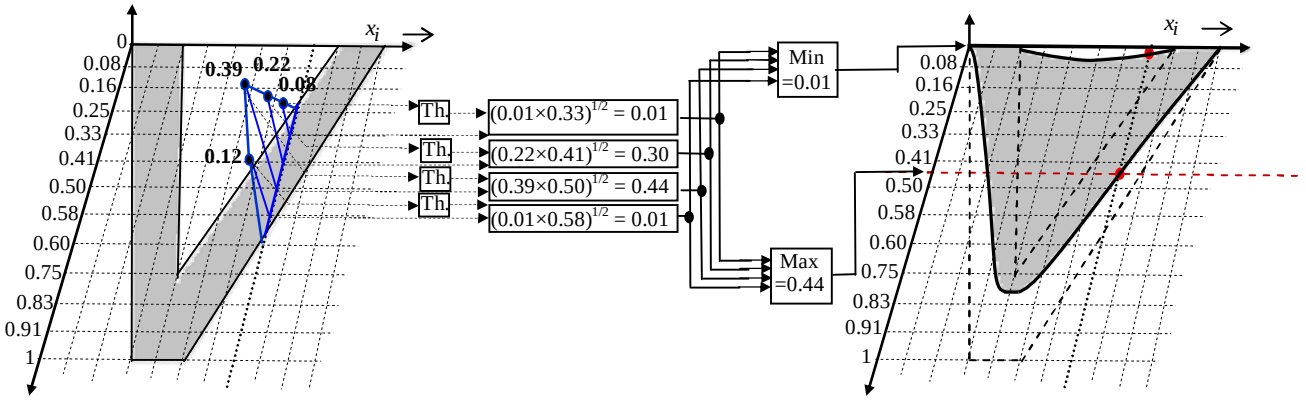

Fig.16 (b) Modified semi-GT2FS FOU for drift in threshold from its optimal value to $th = 0.20$

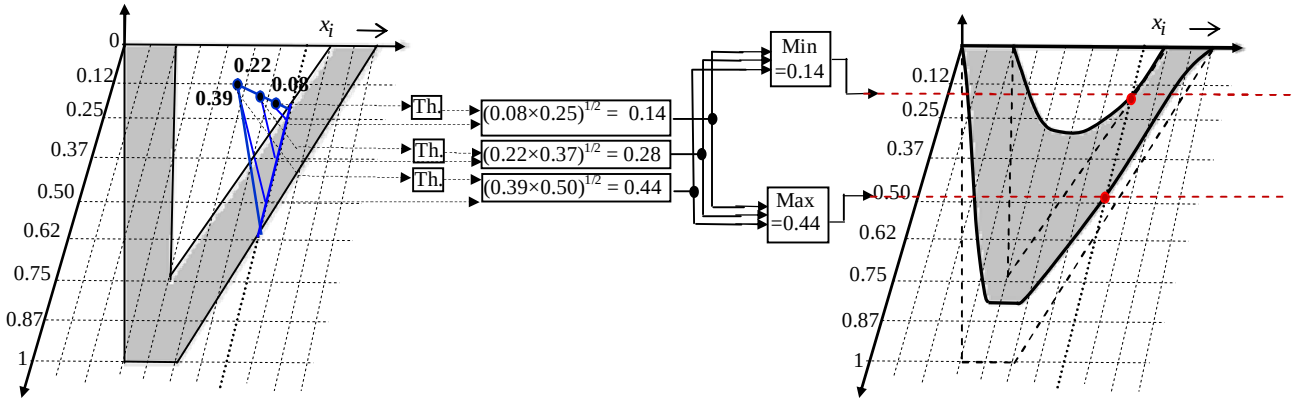

Fig.16 (c) Modified semi-GT2FS FOU for drift in discretization of y-axis from its optimal value to $p = 8$

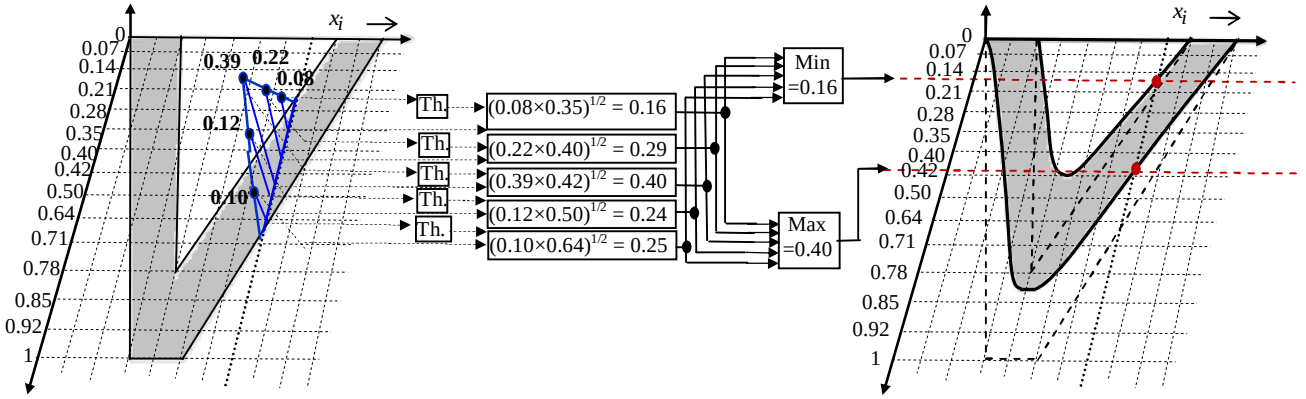

Fig.16 (d) Modified semi-GT2FS FOU for drift in discretization of y-axis from its optimal value to $p = 14$

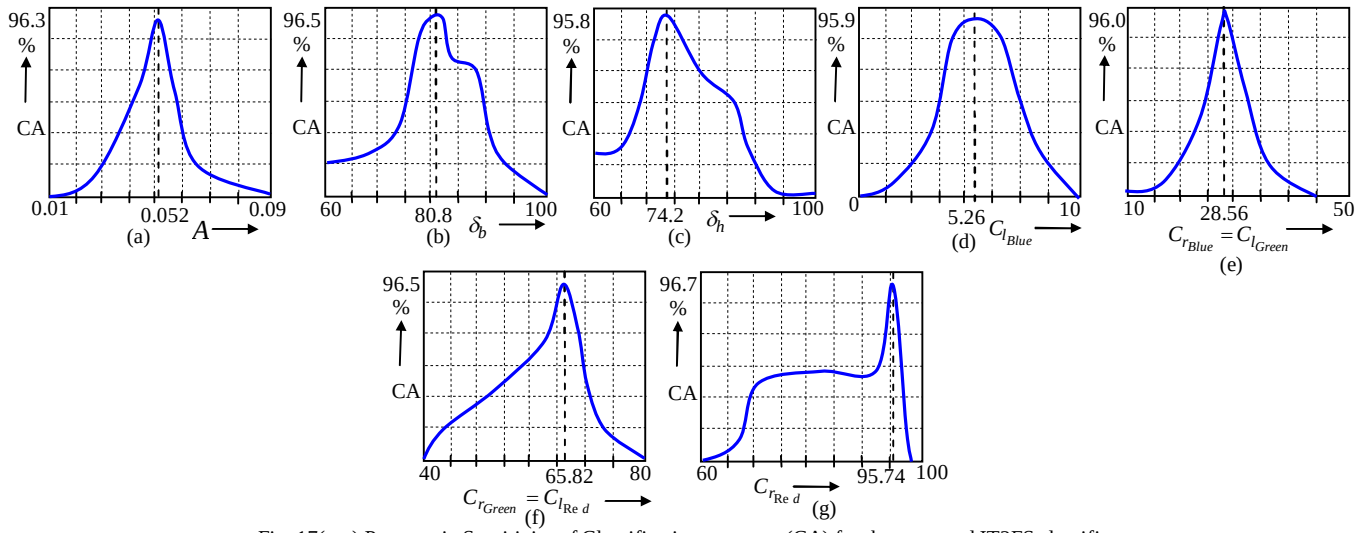

Fig. 17(a-g) Parametric Sensitivity of Classification accuracy (CA) for the proposed IT2FS classifier

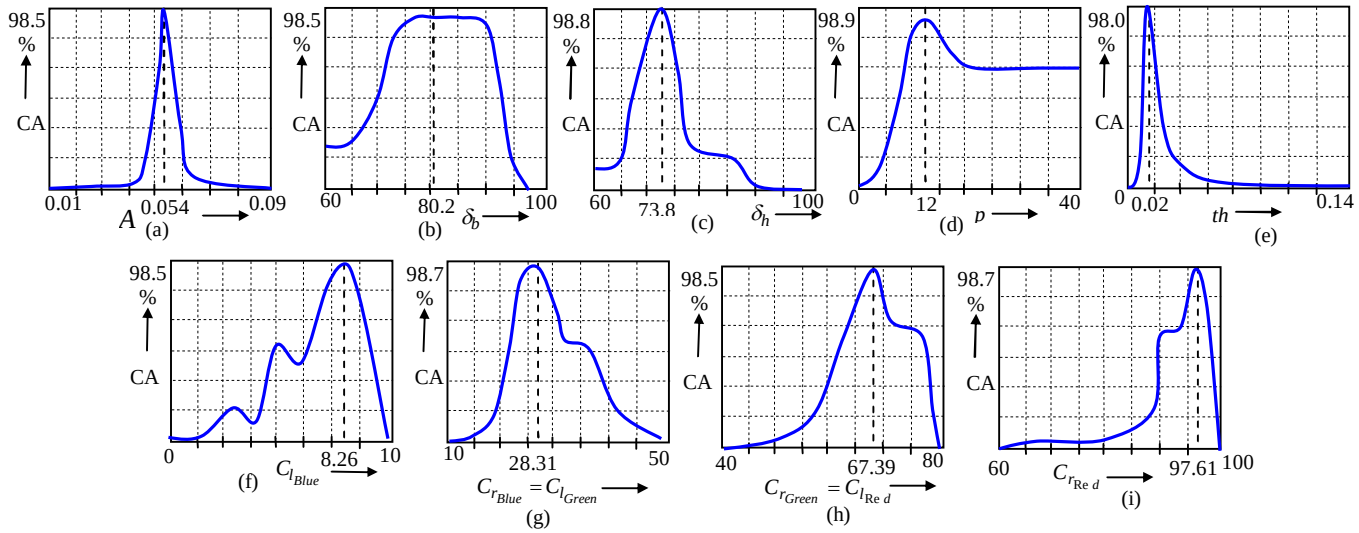

Fig. 18(a-i) Parametric Sensitivity of Classification accuracy (CA) for the proposed Semi- GT2FS classifier

(in Fig. 18(a)-(i)). Here too the results show similar behavior like that of IT2FS.

VII. Classifier Performance and Statistical Analysis

A. *Training Phase*

We examine the classifier performance in two ways, one across different colors and the other by adding colored noise to a selected base color (here, red). We studied individual performance in the training phase and overall performance for different color stimuli in the test phase. Table-II-A and II-B provide the results of performance analysis for the above two cases. It is apparent from Table-II-A that individual class performance is the highest (98.8%) for red and smallest (94.3%) for the golden color with an average of 96.5%. Similarly, in Table-II-B, we varied hue, saturation and brightness over the red color (wavelength 700nm ± 20nm) and noticed that for the chocolate color the performance is the best (97.8%) and worst for the Salmon color (92.7%) with an average classification accuracy of 94.9%.

B. *Test Phase*

To determine the performance in the test phase, we construct confusion matrix (Table- IIIA) to examine the individual color performance. We also determine the tolerance in red, green and blue colors to recognize them correctly for 2 subjects (Table-IIIB). Color tolerance is synthesized by varying hue, saturation and brightness (HSB) around selected center points for the individual base colors. We note that 8 of 10 subjects have narrower tolerance level, but only 2 subjects allowed wider tolerance.

C. *Performance Analysis with/without using PSO*

We study the intra and inter-class performance with/without using PSO. From Table IV, we examine that, the classification accuracy of the noisy color stimulus is increased with introduction of PSO by 6% than the case without PSO.

D. *Proposed Classifier Performance*

The performance of the proposed classifiers has been analyzed at three distinct levels. First, percentage of True

TABLE II-A
CLASSIFICATION ACCURACY FOR TEN STIMULI ACROSS DIFFERENT COLORS AVERAGED OVER 10 SUBJECTS

Stimulus type	Decimal code (R.G,B)	Decimal Code (H, S, B)	Classification Accuracy (in %)		
			Best	Average	Worst
Red	(255,0,0)	(0,240,120)	**98.8**	90.2	85.1
Green	(0,255,0)	(80,240,120)	**96.2**	89.3	80.1
Blue	(0,0,255)	(160,240,120)	**97.4**	91.7	83.8
Brown	(165,42,42)	(0, 143, 97)	**96.5**	90.8	80.7
Orchid	(218,112,214)	(202,141,155)	**95.8**	92.9	84.7
Sea-Green	(254,139,87)	(98,121,87)	**97.9**	87.3	82.6
Royal Blue	(65,105,255)	(152,240,151)	**95.6**	89.4	82.1
Golden	(218,165,32)	(29,179,118)	**94.3**	90.8	81.2

TABLE II-B
CLASSIFICATION ACCURACY FOR THE RED COLOR STIMULI WITH COLORED NOISE AVERAGED OVER 10 SUBJECTS

Color Stimulus type	Decimal code (R,G,B)	Decimal code (H, S, B)	Classification Accuracy (in %)		
			Best	Average	Worst
Firebri—ck	(178,34,34)	(0,163,100)	**96.4**	92.1	82.1
Tomato	(255,99,71)	(6,240,153)	**94.3**	90.6	84.6
Salmon	(250,128,114)	(4,224,171)	**92.7**	91.4	79.5
Indian-red	(205,92,92)	(0,127,140)	**93.5**	88.3	77.1
Choco-late	(210,105,30)	(17,180,113)	**97.8**	84.7	75.2

TABLE III-A
CONFUSION MATRIX OF EIGHT COLOR STIMULI CLASSES USING SEMI-GT2FS CLASSIFIERS

Actual class	Predicted class (in %)							
	Red	Green	Blue	Brown	Orchid	Sea-green	Royal-blue	Golden
Red	96.2	0.00	0.00	1.59	0.85	1.36	0.00	0.00
Green	0.00	97.9	0.00	0.00	0.04	1.26	0.00	0.80
Blue	0.00	0.00	98.6	0.00	0.06	0.00	1.34	0.00
Brown	1.20	0.00	0.00	98.2	0.00	0.60	0.00	0.00
Orchid	0.56	0.00	0.00	0.00	97.3	0.00	1.06	1.08
Sea-Green	0.60	1.60	0.00	0.00	1.00	96.4	0.00	0.40
Royal-Blue	0.00	0.00	0.36	0.00	0.04	1.20	98.4	0.00
Golden	0.00	1.45	0.55	0.00	0.00	0.60	0.00	97.4

TABLE III-B
RECOGNITION TOLERANCE FOR THREE BASIC COLORS OVER 2 SUBJECTS

Subjects	Colors	Range of hue	Range of saturation	Range of brightness
Subject 1	Red	[0-17]	[40-255]	[40-240]
	Green	[47-119]	[82-255]	[53-215]
	Blue	[130-170]	[78-255]	[68-247]
Subject 2	Red	[1-19]	[39-255]	[46-238]
	Green	[45-110]	[80-255]	[50-220]
	Blue	[132-166]	[75-255]	[66-250]

TABLE V
COMPARATIVE STUDY OF THE PROPOSED 2 CLASSIFIERS OVER EXISTING ONES ON JADAVPUR UNIVERSITY DATABASE

CLASSIFIERS	TP%	TN%	FP%	FN%
LSVM [43]	79.0%	78.9%	21.1%	21.0%
KSVM-RBF Kernel [44]	82.7%	80.8%	19.2%	17.3%
KSVM-polynomial Kernel [45]	83.3%	84.6%	15.4%	16.7%
BPNN [46]	87.1%	88.8%	11.2%	12.9%
Type-I Fuzzy	78.1%	76.8%	23.2%	21.9%
IT2FS [47]	90.0%	91.8%	8.2%	10.0%
GT2FS [48]	98.3%	97.0%	3.0%	1.7%
Proposed IT2FS Classifier	95.5%	96.2%	3.8%	4.5%
Proposed Semi-GT2FS	98.9%	97.7%	2.3%	1.1%

Positive (TP), True Negative (TN), False Positive (FP) and False Negative (FN) instances for each class is computed.

TABLE IV
AVERAGE CLASSIFICATION ACCURACY WITH OR WITHOUT PSO

Color Stimulus	Classification Accuracy with PSD + Wavelet EEG Features	
	Without PSO	With PSO
Firebrick	88.4 (0.0128)	**98.5 (0.0100)**
Tomato	82.4 (0.0114)	**98.1 (0.0045)**
Salmon	81.7 (0.0109)	**97.8 (0.0121)**
Indian-red	87.8 (0.0187)	**96.2 (0.0107)**
Chocolate	89.6 (0.0177)	**96.1 (0.0134)**

Table-V provides the results of computation of the percentage of TP, TN, FP and FN instances for the Red color perception, tested on JUDB. It is apparent from Table-V that the proposed Semi-GT2FS classifier out-performs its competitors by a large margin. Second, the classification accuracy for 3 classes is evaluated using expression (27), where,

$$CA = \frac{TP + TN}{TP + TN + FP + FN} \tag{27}$$

is reported in Table-VI. In Table-VI, the relative performance of the proposed 2 classifiers are compared with a few well-known classifiers: Linear Support Vector Machine Classifier (LSVM) [47], Kernelized SVM Radial Basis Function Kernel (KSVM-RBF) [48], KSVM with polynomial kernel

TABLE VI
RELATIVE STUDY OF CLASSIFICATION ACCURACY (STANDARD DEVIATION) FOR BASIC COLORS AND RUNTIME COMPLEXITY

Classifiers	Red	Green	Blue	Run-time complexity (milliseconds)
LSVM [47]	78.9 (0.050)	78.5 (0.056)	79.4 (0.054)	37.15
KSVM-RBF Kernel [48]	81.7 (0.043)	81.1 (0.042)	82.7 (0.030)	44.18
KSVM-polynomial Kernel [49]	83.9 (0.035)	83.8 (0.038)	85.9 (0.031)	44.05
BPNN [50]	87.9 (0.025)	87.9 (0.027)	86.4 (0.028)	110.25
Type-I Fuzzy	77.4 (0.010)	78.8 (0.018)	77.3 (0.017)	31.23
IT2FS [51]	90.9 (0.007)	91.4 (0.006)	91.1 (0.006)	32.76
GT2FS [52]	97.6 (0.005)	97.8 (0.004)	97.9 (0.005)	98.23
Proposed IT2FS Classifier	**95.8 (0.004)**	**96.5 (0.003)**	**96.9 (0.002)**	**32.02**
Proposed Semi-GT2FS	**98.8 (0.003)**	**98.5 (0.002)**	**98.7 (0.001)**	**41.27**

TABLE VIII
PERFORMANCE ANALYSIS USING MCNEMAR'S TEST PERFORMED ON JADAVPUR UNIVERSITY DATABASE WITH SEMI- GT2FS CLASSIFIER AS THE REFERENCE ALGORITHM

Classifier algorithm used for comparison using desired features	Parameter used for Mc Nemar's test		z	Comments on acceptance/rejection of hypothesis
	m_{01}	m_{10}		
LSVM	20	63	21.2	Reject
KSVM-RBF Kernel	17	67	28.5	Reject
KSVM-polynomial Kernel	5	14	3.68	Accept
BPNN	23	49	8.68	Reject
Type-I Fuzzy	31	97	33.0	Reject
IT2FS [51]	12	4	3.06	Accept
GT2FS [52]	7	16	2.78	Accept
Proposed IT2FS	9	18	2.37	Accept

(KSVM-Polynomial) [49], Back- propagation Neural Net (BPNN) [50], Type-1 fuzzy, Classical IT2FS [51] GT2FS - based classifiers [52] with respect to classification accuracy and runtime. It is apparent from the Table that the proposed semi-GT2FS classifier outperforms the traditional ones by a large margin, leaving with respect to both classification accuracy and runtime. The proposed IT2FS classifier too provides very high classification accuracy at significantly low run-time complexity. Lastly, the classification accuracy of the proposed 2 techniques are compared with three databases, i.e.: JUDB, SWBDB and NIDB. It is apparent from the Table-VII that the classification accuracy of semi-GT2FS algorithm outperforms the former proposed IT2FS classifiers over three different datasets.

TABLE VII
PERCENTAGE CLASSIFICATION ACCURACY AVERAGED OVER 3 CLASSES OF OUR PROPOSED METHOD OVER THREE DATABASES

CLASSIFIERS	JUDB [37]	SWBDB [38]	NIDB [39]	Averaged Accuracy over Last 3 Columns
PROPOSED IT2FS	96.2%	95.1%	96.2%	96.2%
PROPOSED SEMI-GT2FS	98.5%	97.4%	98.3%	98.1%

TABLE IX
STATISTICAL COMPARISON OF PERFORMANCE USING MC. NEMAR'S TEST WITH THREE DATABASES

Reference Algorithm: Semi- GT2FS classifier						
Classifier algorithm used for comparison using desired features	JUDB [37]		SWBDB [38]		NIDB [39]	
	z-score	Comments on acceptance/rejection of hypothesis	z-score	Comments on acceptance/rejection of hypothesis	z-score	Comments on acceptance/rejection of hypothesis
LSVM	21.2	Reject	2.91	Accept	31.2	Reject
KSVM-RBF Kernel	28.5	Reject	28.5	Reject	11.8	Reject
KSVM-polynomial Kernel	3.68	Accept	3.31	Accept	2.87	Accept
BPNN	8.68	Reject	1.68	Accept	15.7	Reject
Type-I Fuzzy	33.0	Reject	8.47	Reject	24.9	Reject
IT2FS [51]	3.06	Accept	3.02	Accept	3.41	Accept
GT2FS [52]	2.78	Accept	2.54	Accept	2.86	Accept
Proposed IT2FS	2.37	Accept	1.97	Accept	2.10	Accept

TABLE X
AVERAGE RANKING OF CLASSIFICATION ALGORITHMS BY FRIEDMAN TEST

Classifier Algorithms	Rank obtained though experiments with database			Average Rank
	JUDB [37]	SWBDB [38]	NIDB [39]	
LSVM	9	9	9	9
KSVM-RBF Kernel	6	8	7	7
KSVM-polynomial Kernel	4	6	8	6
BPNN	7	7	6	6.66
Type-I Fuzzy	8	4	3	5
IT2FS [51]	3	5	5	4.33
GT2FS [52]	5	2	4	3.66
Proposed IT2FS	2	3	2	2.33
Proposed Semi-GT2FS	1	1	1	1

E. Statistical Tests

We adopted McNemar's test [53] to statistically test and validate the proposed classifiers against the standard ones. Table-VIII has been constructed to undertake the test. Here, we consider two classifiers X and Y, where the former is realized with Semi-GT2FS algorithm and the latter by one of the 8 algorithms respectively. Let m_{01} be the number of

TABLE XI
COLOR PERCEPTUAL –ABILITY ANALYSIS FOR TEN SUBJECTS

Subject	ARP	RT	PA (ARP×RT)	% of PA	Rank
1	0.824	0.39	0.321	32.1	9
2	0.749	0.57	0.426	42.6	7
3	0.766	0.36	0.275	27.5	10
4	0.861	0.48	0.413	41.3	8
5	0.895	0.82	0.733	73.3	2
6	**0.901**	**0.92**	**0.828**	**82.8**	**1**
7	0.847	0.67	0.567	56.7	5
8	0.834	0.58	0.483	48.3	6
9	0.815	0.76	0.619	61.9	4
10	0.899	0.81	0.728	72.8	3

classes misclassified by X but not by Y. Similarly, let m_{10} be the number of classes misclassified by Y but not by X. Then, we define a statistic

$$z = \frac{(|m_{01} - m_{10}| - 1)^2}{m_{01} + m_{10}} \tag{28}$$

According to the χ^2 distribution table, we have $\chi^2_{1,0.95} = 3.84$ represents the value of Chi-square with probability 0.05 and the degree of freedom 1. The null hypothesis, representing that the two classifiers have identical performance with respect to the given classifier accuracy, is rejected as z exceeds $\chi^2_{1,0.95} = 3.84$.

The statistical comparisons of three databases are performed in Table IX. It is evident from the Table that McNemar's test is unable to detect the superiority of an algorithm over others. Thus Friedman Test is required to rank the above algorithms.

F. Friedman Test

Friedman test [54] provides an additional merit over McNemar's test to rank the individual algorithms based on each data set separately. The algorithm having the best performance is assigned rank 1. The average of the ranks attained by each algorithm across all databases is evaluated for evaluation of the Friedman statistic χ^2_F.

Let $r_{a,b}$ be the rank of the algorithm *a*'s on the *b*-th dataset. The average rank of the algorithm '*a*' is evaluated by

$$R_a = \frac{1}{N} \sum_{\forall b} r_{a,b}, \tag{29}$$

where *N* (=3, here) denotes the number of datasets. The null hypothesis indicates that all the algorithms used for comparison are equivalent; hence their respective ranks R_a must be equal. Here, the percentage classification accuracy of the algorithms is considered as the basis of the ranks. The Friedman static χ^2_F of (k-1) degrees of freedom is given by

$$\chi^2_F = \frac{12N}{k(k+1)} \left[\sum_a R_a^2 - \frac{k(k+1)^2}{4} \right]. \tag{30}$$

With k=9 and N=3 and using the average ranks from Table-X, we obtain $\chi^2_F = 19.48 > \chi^2_{8,\,0.95} = 15.51$. Here, $\chi^2_{8,0.95} = 15.51$ depicts the value of chi square distribution for 8 degree of freedom at the probability of 0.05. Consequently, the null hypothesis that all the algorithms are equivalent is ejected. So, the performance of the algorithms should be compared by their ranks only.

It is apparent from Table-X that the average rank of the proposed Semi-GT2FS classifier is 1, signifying that Semi-GT2FS outperforms all the algorithms by Friedman Test.

G. Ranking Color Perceptual-Ability of Subjects

To rank subjects based on color perceptual-ability, we undertake 3 steps. First, we compute ARP and RT for 30 subjects, of which only 10 are shown in Table-XI for space limitation. Second, we take their product to compute perceptual-ability of the individual subjects. Lastly, we sort the subjects based on the descending order of their perceptual-ability. The ranks of the subjects thus obtained are indicated in the Table itself.

VIII. CONCLUSION

This paper introduces a novel approach to measure the color perceptual-ability of subjects from their EEG response. The PSD and Wavelet coefficients are extracted from the EEG response to color stimuli acquired from the activated brain regions, identified by e-LORETA. A novel semi-GT2FS fuzzy classifier that takes care of secondary memberships but works similar to IT2FS with significantly reduced computational overhead has been employed to classify the colors perceived by the subjects. Performance analysis undertaken with respect to classification accuracy indicates that the proposed Semi-GT2FS classifier outperforms all the existing classifiers by a significant margin. Statistical tests undertaken also confirm the same results. The proposed technique has interesting application in chemical, pharmaceutical and textile industries, particularly to rank candidates based on their color perceptual-ability for possible appointment in the company.

ACKNOWLEDGMENT

The authors gratefully acknowledge the financial support they received from the University Grants Commission (UGC) sponsored *UPE-II project in Cognitive Science*, and the Ministry of Human Resource Development (MHRD) sponsored *JU-RUSA 2.0* project allocated to Jadavpur University, Kolkata-700 032, India.

REFERENCES

[1] Edwin H Land, (1983): "Recent advances in retinex theory and some implications for cortical computations: color vision and the natural image," *Proceedings of the National Academy of Sciences*, vol. 80, no. 16, pp. 5163-5169, 1983.

[2] Edward A. Essock, J. Sinai Michael, S. McCarley Jason, K. Krebs William, and J. Kevin DeFord, "Perceptual ability with real-world nighttime scenes: image-intensified, infrared, and fused-color imagery," *Human Factors*, vol. 41, no. 3, pp.438-452, 1999.

[3] J. Kroneg, C. Guillaume, V. Sviatoslav, and P. Thierry, "EEG-based synchronized brain-computer interfaces: A model for optimizing the

number of mental tasks," *IEEE Trans. Neural Systems and Rehabilitation Engineering*, vol. 15, no. 1, pp.50-58, 2007.

[4] S. Zeki, and M. Ludovica, "Three cortical stages of colour processing in the human brain," *Brain: a journal of neurology*, vol. 121, no. 9, pp. 1669-1685, 1998.

[5] G. J. Brouwer, and J. H. David, "Decoding and reconstructing color from responses in human visual cortex," *J. of Neuroscience*, vol. 29, no. 44, pp.13992-14003, 2009.

[6] R. W. Homan, H. John, and P. Phillip, "Cerebral location of international 10–20 system electrode placement," *Electroencephalography and clinical neurophysiology*, vol. 66, no. 4, pp. 376-382, 1987.

[7] L. Canuet, I. Ryouhei i, D. Pascual-M. Roberto, I. Masao, K. Ryu, A. Yasunori, I. Shunichiro, T. Hidetoshi, N. Takayuki, and T. Masatoshi, "Resting-state EEG source localization and functional connectivity in schizophrenia-like psychosis of epilepsy," *PloS one*, vol. 6, no. 11, pp. e27863, 2011.

[8] R. D. Pascual-Marqui, D. Lehmann, T. Koenig, K. Kochi, M. C. Merlo, D. Hell, & M. Koukkou, "Low resolution brain electromagnetic tomography (LORETA) functional imaging in acute, neuroleptic-naive, first-episode, productive schizophrenia," *Psychiatry Research: Neuroimaging*, vol. 9, no. 3, pp. 169-179, 1999.

[9] A.Yoto, T. Katsuura, K. Iwanaga, and Y. Shimomura, "Effects of object color stimuli on human brain activities in perception and attention referred to EEG alpha band response", J. *of Physiological Anthropology*, vol. 26, no. 3, pp. 373-379, 2007.

[10] A. Y. Kaplan, J. G. Byeon, J. J. Lim, K. S. Jin, B. W. Park, and S. U. Tarasova, "Unconscious operant conditioning in the paradigm of brain-computer interface based on color perception," *International journal of neuroscience*, vol. 115, no. 6, pp.781-802, 2005.

[11] Anna Franklin, *et al.*, "Color perception in children with autism. Journal of Autism and Developmental Disorders," *J. Autism Dev Disord, vol.* 38, no. 10, pp. 1837-1847, 2008.

[12] O. Olurinola, and O. Tayo, (2015). "Colour in Learning: Its Effect on the Retention Rate of Graduate Students," *J. of Education and Practice*, vol. *6*, no. 14, pp. 1-5, 2015.

[13] M. Olkkonen, and S. R. Allred, "Short-term memory affects color perception in context," *PloS one*, vol. *9, no.*1, pp. e86488, 2014.

[14] A. U. Viola, L. M. James, L. J. Schlangen, and D. J. Dijk, "Blue-enriched white light in the workplace improves self-reported alertness, performance and sleep quality," *Scandinavian journal of work, environment and health*, pp. 297-306, 2008.

[15] M. J. Goard, G. N. Pho, J. Woodson, and M. Sur, "Distinct roles of visual, parietal, and frontal motor cortices in memory-guided sensorimotor decisions," *Elife*, *5*, 2016.

[16] N. N. Karnik, J. M. Mendel, and Q. Liang, "Type-2 fuzzy logic systems," *IEEE transactions on Fuzzy Systems*, vol:7, No. 6, pp.643-658, 1999.

[17] J. M. Mendel and R. I. B. John, "Type-2 Fuzzy Sets Made Simple", *IEEE Transactions on fuzzy systems*, vol. 10, no. 2, pp; 117-127, 2002.

[18] J. M. Mendel, R. I. John, and F. Liu, "Interval type-2 fuzzy logic systems made simple," *IEEE Trans. Fuzzy Systems*, vol. 14, no. 6, pp. 808-821, 2006.

[19] J. M. Mendel, "General type-2 fuzzy logic systems made simple: a tutorial," *IEEE Trans. Fuzzy Systems*, vol. 22, no. 5, pp. 1162-1182, 2014.

[20] J. M. Mendel, M. R. Rajati and P. Sussner, "On clarifying some definitions and notations used for type-2 fuzzy sets as well as some recommended changes", *Information Sciences*, pp. 337-345 , 2016.

[21] D. Wu and J. M. Mendel, "Enhanced Karnik-Mendel Algorithms," IEEE Trans. Fuzzy Systems, vol. 17, no.4, pp. 923-934, Aug. 2009.

[22] A. Kachenoura, L. Albera, L. Senhadji, and P. Comon, "ICA: a potential tool for BCI systems," *IEEE Signal Processing Mag*., vol. 25, no. 1, pp. 57-68, 2008.

[23] P. Herman, G. Prasad, T. M. McGinnity, and D. Coyle, "Comparative analysis of spectral approaches to feature extraction for EEG-based motor imagery classification," *IEEE Trans. Neural Systems and Rehabilitation Engineering*, vol. *16, no*. 4, pp. 317-326, 2008.

[24] M. M. H. Chowdhury and A. Khatun, "Image compression usingdiscrete wavelet transform," *IJCSI International Journal of Computer Science Issues*, vol. *9*, no. 4, pp. 327-330, 2012.

[25] V. S. Devi and M. N. Murty, *Pattern Recognition-: An introduction*. India: Hydrabad,Univ. Press, 2011.

[26] Q. Du, H. Yang, and N. H. Younan, "Improved sequential endmember extraction algorithms," in Proc. IEEE Conf. Hyperspectral Image Signal *Process.: Evolution Remote Sensing*, Lisbon, Portugal, Jun. 2011, pp. 1–4.

[27] S. Das, A. Abraham, and A. Konar, "Particle swarm optimization and differential evolution algorithms: technical analysis, applications and hybridization perspectives," *In Advances of computational intelligence in industrial systems, Springer, Berlin, Heidelberg*, pp. 1-38, 2008.

[28] S. Das, A. Konar, and U. K. Chakraborty, "Improving particle swarm optimization with differentially perturbed velocity," In Proc. of *the 7th annual conference on Genetic and evolutionary computation, ACM*, pp. 177-184, June 2005.

[29] G. J. Klir and B. Yuan, *Fuzzy Sets and Fuzzy Logic: Theory and Application*. Englewood Cliffs, NJ, USA: Prentice-Hall, 1997.

[30] J. Aisbett, and J. T. Rickard, (2014). "Centroids of type-1 and type-2 fuzzy sets when membership functions have spikes," *IEEE Trans. Fuzzy Systems*, vol. 22, no. 3, pp. 685-692, 2014.

[31] D. Wu, "A constrained representation theorem for interval type-2 fuzzy sets using convex and normal embedded type-1 fuzzy sets and its application to centroid computation," In Proc. of *World Conference on Soft Computing, San Francisco, CA*, May 2011.

[32] M. Pratama, J. Lu, E. Lughofer, G. Zhang, and S. Anavatti, "Scaffolding type-2 classifier for incremental learning under concept drifts," *Neurocomputing*, vol. 191, pp. 304–329, 2016.

[33] M. A. Sanchez, O. Castillo, and J. R. Castro,"Generalized type-2 fuzzy systems for controlling a mobile robot and a performance comparison with interval type-2 and type-1 fuzzy systems,". *Expert Systems with Applications*, vol. *42, no.* 14, pp. 5904-5914, 2015.

[34] C. Wagner, and H. Hagras. "Toward general type-2 fuzzy logic systems based on zSlices," *IEEE Trans. Fuzzy Systems*, vol. 18, no. 4, pp. 637-660, 2010.

[35] H. Levkowitz, & G. T. Herman, "GLHS: A generalized lightness, hue, and saturation color model," *Graphical Models and Image Processing*, vol. 55, no. 4, pp. 271-285, 1993.

[36] S. Lall, A. Saha, A. Konar, M. Laha, A. L. Ralescu, K. M. kumar and A. K . Nagar, "EEG-based mind driven type writer by fuzzy radial basis function neural classifier," In *Neural Networks (IJCNN), 2016 International Joint Conference* on IEEE, pp. 1076-1082, July 2016.

[37] A. Saha, A. Konar, A. Chatterjee, A. L. Ralescu & A. K. Nagar, "EEG analysis for olfactory perceptual-ability measurement using recurrent neural classifier," *IEEE Trans. Human-machine systems*, vol. 44, no. 6, pp. 717-730, Dec. 2014.

[38] A. Khasnobish, A. Konar, D. Tibrewala, and A. K. Nagar, "Bypassing the natural visual motor pathway to execute complex movement related tasks using interval type-2 fuzzy sets", *IEEE Trans. Neural System and Rehabilation Engineering*, vol. 25, no. 1, 2017,pp.88-102.

[39] Jadavpur University Database for Color Perception, prepared at Artificial Intelligence Lab., ETCE Dept., Jadavpur University, 2019. [Online]. Available: http://amitkonar.com/tcds/howtoreadJUDbase.pdf; http://amitkonar.com/tcds/JUDbase.zip

[40] South-West Bengal Database for Color Perception, prepared at Artificial Intelligence Lab., ETCE Dept., Jadavpur University, 2019. [Online]. Available: http://amitkonar.com/tcds/howtoreadSWBDbase.pdf;

http://amitkonar.com/tcds/SWBDbase.zip

[41] North-Indian Database for Color Perception, prepared at Artificial Intelligence Lab., ETCE Dept., Jadavpur University, 2019. [Online]. Available: http://amitkonar.com/tcds/howtoreadNIDbase.pdf; http://amitkonar.com/tcds/NIDatabase.zip

[42] M. Hata, H. Kazui, T. Tanaka, R. Ishii, L. Canuet, R. D. Pascual-Marqui, Y. Aoki, S. Ikeda, H. Kanemoto, K. Yoshiyama, and M. Iwase, "Functional connectivity assessed by resting state EEG correlates with cognitive decline of Alzheimer's disease–An eLORETA study," *Clinical Neurophysiology*, vol. 127, no. 2, pp.1269-1278, 2016.

[43] A. Saha, A. Konar, and A. K. Nagar. "EEG Analysis for Cognitive Failure Detection in Driving Using Type-2 Fuzzy Classifiers," *IEEE Trans. Emerging Topics in Computational Intelligence*, vol. 1, no. 6, pp. 437-453, 2017.

[44] P. Rakshit, A. Konar, S. Das, L. C. Jain, A. K. Nagar, "Uncertainty management in differential evolution induced multiobjective optimization in presence of measurement noise," IEEE Transactions on Systems, Man, and Cybernetics: Systems, vol. 44, no. 7, pp. 922-937, 2013.

[45] S. Das, A. Abraham, and A. Konar, "Automatic clustering using an improved differential evolution algorithm," *IEEE Trans. on systems, man, and cybernetics-Part A: Systems and Humans*, vol. 38, No. 1, pp. 218-237, 2007.

[46] M. Ataei,and M. Osanloo, "Using a combination of genetic algorithm and the grid search method to determine optimum cutoff grades of multiple metal deposits," *International Journal of Surface Mining, Reclamation and Environment*, vol. 18, no. 1, pp: 60-78, 2004.

[47] F. Pan, B. Wang, X. Hu, & W. Perrizo, "Comprehensive vertical sample-based KNN/LSVM classification for gene expression analysis," *J. of Biomedical Informatics*, vol. 37, no. 4, pp. 240-248, 2004.

[48] U. Ravale, N. Marathe, and P. Padiya, "Feature selection based hybrid anomaly intrusion detection system using K means and RBF kernel function," *Procedia Computer Science*, vol. 45, pp. 428-435, 2015.

[49] X. Kejia, T. Zhiying, and C. Bin, "Reweighting Recognition Using Modified Kernel Principal Component Analysis via Manifold Learning," In *Advanced Technology in Teaching-Proceedings of the 2009 3rd International Conference on Teaching and Computational Science (WTCS 2009)*, Springer, Berlin, Heidelberg, pp. 609-617, 2012.

[50] V.N.P. Rao, and Rao Vemuri, "A Performance Comparison of Different Back Propagation Neural Networks Methods in Computer Network Intrusion Detection,"

[51] A. Halder, A. Konar, R. Mandal, A. Chakraborty, P. Bhowmik, N. R. Pal, and A. K. Nagar, "General and interval type-2 fuzzy face-space approach to emotion recognition," *IEEE Trans. Systems, Man, and Cybernetics: Systems, vol.* 43, no. 3, pp. 587-605, 2013.

[52] A. Halder, R. Mandal, A. Chakraborty, A. Konar, and R. Janarthanan, "Application of general type-2 fuzzy set in emotion recognition from facial expression," In *International Conference on Swarm, Evolutionary, and Memetic Computing, Springer, Berlin, Heidelberg*, pp. 460-468, Dec. 2011.

[53] X. Sun, Z. Yang, " Generalized McNemars Test for Homogeneity of the marginal distribution," , in proc. of *SAS global Forum*, paper 382, 2006.

[54] J. Demsar, "Statistical comparisons of classifiers over multiple data sets," J. Mach. Learn. Res., vol. 7, pp. 1–30, Dec. 2006.

Mousumi Laha received her B.Tech. degree in Electronics and Tele-Communication Engineering from Camellia Institute of Technology in 2011, and her M. Tech. degree in Intelligent Automation and Robotics (IAR) from the department of Electronics and Tele-Communication Engineering, Jadavpur University, Kolkata in 2015. She is currently pursuing her Ph.D. in Cognitive Intelligence in Jadavpur University under the guidance of Prof. Amit Konar and Dr. Pratyusha Rakshit. Her current research interest includes type-2 fuzzy sets, brain-computer interfaces, and biological underpinning of cognition and sensory perception.

Amit Konar (SM' 2010) is currently a Professor in the department of Electronics and Tele-Communication Engineering, Jadavpur University, Kolkata, India. He earned his B.E. degree from Bengal Engineering College, Sibpur in 1983, and his M.E., M. Phil. and Ph.D. degrees, all from Jadavpur University in 1985, 1988 and 2004 respectively. Dr. Konar has published 15 books and over 350 research papers in leading international journals and conference proceeding. He has supervised 28 PhD theses and 262 Masters' theses. He is a recipient of AICTE-accredited Career Award for Young Teachers for the period: 1997-2000. He is nominated as a Fellow of West Bengal Academy of Science and Engineering in 2010 and (Indian) National Academy of Engineering in 2015. Dr. Konar has been serving as an Associate Editor of several international journals, including IEEE Transactions of Fuzzy Systems and IEEE Transactions of Emerging Trends in Computational Intelligence. His current research interest includes Cognitive Neuroscience, Brain-Computer Interfaces, Type-2 Fuzzy Sets and Multi-agent Systems.

Pratyusha Rakshit received the B. Tech. degree in Electronics and Communication Engineering (ECE) from Institute of Engineering and Management, India, and M.E. degree in Control Engineering from Electronics and Telecommunication Engineering (ETCE) Department, Jadavpur University, India in 2010 and 2012 respectively. She was awarded her Ph.D. (Engineering) degree from Jadavpur University, India in 2016. From August 2015 to November 2015, she was an Assistant Professor in ETCE Department, Indian Institute of Engineering Science and Technology, India. She is a permanent faculty in the rank of Assistant Professor in ETCE Department, Jadavpur University. Currently, she is on lien to purue her post-doctoral research to Basque Center for Applied Mathematics, Bilbao,Spain. She was awarded Gold Medals for securing the highest percentage of marks in B. Tech. in ECE and among all the courses of M.E. respectively in 2010 and 2012. She was the recipient of CSIR Senior Research Fellowship, INSPIRE Fellowship and UGC UPE-II Junior Research Fellowship. Her principal research interests include artificial and computational intelligence, evolutionary computation, robotics, bioinformatics, pattern recognition, fuzzy logic, cognitive science and human-computer interaction. She is an author of over 50 papers published in top international journals and conference proceedings. She serves as a reviewer in IEEE-TFS, IEEE-SMC: Systems, Neurocomputing, Information Sciences, and Applied Soft Computing.

Atulya K. Nagar holds the Foundation Chair as Professor of Mathematical Sciences at Liverpool Hope University where he is the Dean of the Faculty of Science. He received a prestigious Commonwealth Fellowship for pursuing his Doctorate (DPhil) in Applied Non-Linear Mathematics, which he earned from the University of York in 1996. Prior to joining Liverpool Hope, he was with the Department of Mathematical Sciences, and later at the Department of Systems Engineering, at Brunel University, London. His research is inter-disciplinary with expertise in Nonlinear Mathematics, Natural Computing, Bio-Mathematics and Computational Biology, as well as Control Systems Engineering. He has edited volumes on Intelligent Systems, and Applied Mathematics. He is the Editor-in-Chief of the International Journal of Artificial Intelligence and Soft Computing (IJAISC) and serves on editorial boards for a number of prestigious journals. He is well published with over 400 publications in prestigious publishing outlets such as the *Journal of Applied Mathematics and Stochastic Analysis*, the *International Journal of Foundations of Computer Science*, *the IEEE Transactions, Discrete Applied Mathematics, Fundamenta Informaticae, IET Control Theory & Applications* and others. Prof Nagar is a Chair of University's Research Committee including Research Excellence Framework (REF) and sits on a number of strategic UK wide research bodies including the JISC.